Dynamic CO_2 evasion and colloidal control of trace metals in the Lower Lena River

Yuri Ya. Kolesnichenko[1], Sergey N. Vorobyev[1], Viktor A. Nikitkin[1], Oleg V. Dudarev[2], Denis V. Chernykh[2,3], Eduard A. Spivak[2,3], Arkadiy V. Kurilenko[2,3], Vladimir A. Kholodov[2], Igor P. Semiletov[2,3], Oleg S. Pokrovsky[4,5*]

[1]National Research Tomsk State University (TSU), Lenina Ave., 36, Tomsk, 634050, Russia
[2]V.I. Il'ichev Pacific Oceanological Institute Far Eastern Branch Russian Academy of Science, Baltiyskaya st., 43, Vladivostok, 690041, Russia
[3]Sakhalin State University (SakhGU), Yuzhno Sakhalinsk , Russia
[4]Geosciences and Environment Toulouse, UMR 5563 CNRS, 14 Avenue Edouard Belin 31400 Toulouse, France
[5]N. Laverov Federal Center for Integrated Arctic Research, Russian Academy of Sciences, Arkhangelsk, Russia

Key words: carbon, emission, permafrost, major elements, trace elements, Siberia

* email: oleg.pokrovski@cnrs.fr

Abstract

Large Arctic rivers integrate carbon and element fluxes across vast permafrost-dominated landscapes, yet the lower reaches of these systems remain poorly constrained in terms of greenhouse gas (GHG) emissions and solute distributions. We investigated the Lower Lena River over ~1500 km during the beginning of summer baseflow, combining continuous in situ pCO_2 measurements, floating chamber flux determinations, and analyses of major and trace elements including colloidal size fractionation. pCO_2 exhibited pronounced short-distance variability and decreased weakly northward along the main stem. Diffusive CO_2 fluxes (0.1–1.3 g C m^{-2} d^{-1}) were comparable to values reported for other large Siberian rivers, confirming the Lena as a persistent but moderate atmospheric CO_2 source during the open-water season. In contrast, CH_4 concentrations were low and spatially uniform, contributing <0.5% to total carbon emissions. Notably, bulk DOC and DIC concentrations remained remarkably stable along the transect and were consistent with long-term monitoring records and previous expeditions, indicating stability of bulk dissolved carbon concentrations despite dynamic CO_2 evasion.

Dissolved (< 0.45 µm) major and trace elements formed two major geochemical groups. Highly mobile major ions, Si, and selected oxyanion-forming trace elements were predominantly present in low molecular weight (< 1 kDa) form (0–20% colloidal fraction) and reflected groundwater connectivity and water–rock interaction. In contrast, lithogenic low-solubility elements—including trivalent and tetravalent hydrolysates—were strongly associated with Fe–Al–organic colloids (>70%), indicating surface and suprapermafrost mobilization pathways. Multivariate statistics confirmed this dual organization of solute transport. These findings indicate a functional decoupling between stable bulk dissolved-carbon concentrations and dynamically regulated CO_2 exchange, a pattern likely characteristic of large Arctic rivers. Under ongoing warming, shifts in hydrological connectivity, discharge regime, and permafrost thaw may alter this balance, with implications for pan-Arctic carbon and element export to the Arctic Ocean.

Introduction

Greenhouse gas (GHG) emissions from inland waters in permafrost-affected regions constitute a critical component of the Arctic carbon cycle and represent one of the most important positive feedbacks to ongoing climate warming (Schuur et al., 2015). Permafrost thaw mobilizes large reservoirs of previously frozen organic carbon (OC), increasing its susceptibility to microbial degradation and atmospheric release, or promoting its lateral export to rivers and lakes (Frey and Smith, 2005; Vonk et al., 2019). Once transferred to aquatic systems, this carbon can be rapidly mineralized to CO_2 and CH_4 or transported downstream to the Arctic Ocean. In addition, macro- and micronutrients can be released from progressively thawing soils via surface flow or enhanced underground influx due to increasing connectivity with deep reservoirs, thereby affecting coastal productivity and exerting biogeochemical control at the land – ocean interface (Frey et al., 2007; Tank et al., 2023).

For these reasons, the biogeochemistry of dissolved organic carbon, major ions, and trace elements in Arctic rivers has been intensively investigated (Gordeev et al., 1996, 2004; Holmes et al., 2000, 2001; Tank et al., 2012; Drake et al., 2018; Kipp et al., 2020; Pipko et al., 2023; Savenko and Savenko, 2024). Numerous studies have constrained seasonal export fluxes of dissolved and particulate constituents in major rivers (Holmes et al., 2012; Gordeev et al., 2024; Juhls et al., 2025), as well as in mid-sized fluvial systems and tributaries (Chupakov et al., 2020, 2023; Pokrovsky et al., 2010, 2022; Bagard et al., 2011; Krickov et al., 2025). These efforts have clarified how hydrological regime, permafrost thaw, and watershed characteristics regulate solute mobilization. However, much less attention has been paid to the spatial variability of CO_2 and CH_4 within river networks, and to their coupling to other hydrochemical parameters and landscape structure during open-water period. Furthermore, although this land–water–atmosphere continuum is widely recognized, *in situ* data on GHG concentrations and emissions from major Siberian rivers—particularly during hydrologically dynamic periods—remain scarce.

Among the six great Arctic rivers, the Lena River is particularly emblematic. Draining nearly 2.5 million km² and flowing almost entirely within the continuous permafrost zone, it exhibits extreme seasonal discharge variability and documented increases in annual runoff (Yang et al., 2002; McClelland et al., 2004; Smith and Pavelsky, 2008; Ahmed et al., 2020). The basin encompasses extensive peatlands and yedoma deposits rich in ancient OC that are increasingly affected by thaw (Zhang et al., 2005; Wild et al., 2019). These landscapes provide both modern and aged carbon to aquatic systems, potentially enhancing in-river GHG production during periods of intense lateral connectivity. While Lena River discharge (Berezovskaya et al., 2005; Ye et al., 2009; Tananaev et al., 2016; Gautier et al., 2018; Suzuki et al., 2018; Tananaev and Lotsari, 2022), sediment transport (Rachold et al., 1996; Dudarev et al., 2006), OC dynamics (Lara et al., 1998; Semiletov et al., 2011; Gonçalves-Araujo et al., 2015; Griffin et al., 2018; Ogneva et al., 2023), and hydrochemistry (Gordeev and Sidorov, 1993; Huh et al., 1998a, b; Huh and Edmond, 1999; Georgiadi et al., 2019; Juhls et al., 2020) have been extensively documented, direct assessments of in-situ CO_2 and CH_4 concentrations and emissions along the main stem and its tributaries remain fragmentary. Existing GHG studies are largely confined to the Lena Delta (Kutzbach et al., 2007; Franz et al., 2016; Eckhardt et al., 2019; Beckebanze et al., 2022; Wegner et al., 2022) or upper reaches south of the Aldan River (Vorobyev et al., 2021a, b), leaving the 1200-km middle reach between Yakutsk and Kyusyur and several major tributaries (Vilyui, Muna, Molodo, Kyusyur) poorly constrained. This contrasts with more spatially integrated assessments conducted for the Yukon (Striegl et al., 2012), Mackenzie (Horan et al., 2019), and Ob (Pipko et al., 2019; Karlsson et al., 2021; Vorobyev et al., 2024).

Here, we provide a quantitative assessment of CO_2 and CH_4 concentrations and diffusive emissions along the Lower Lena River main stem and key tributaries during the post-freshet recession, a period of high hydrological connectivity and lateral carbon transfer. The novelty of this work lies in combining high-resolution longitudinal pCO_2 observations and chamber-based fluxes with major and trace solute chemistry and operational colloidal fractionation within the same hydrological period. This integrated approach allows us to evaluate whether tributaries act as localized modulators of greenhouse-gas exchange and whether CO_2 evasion is linked to DOC, DIC, major ions, and trace-element partitioning. By coupling gas fluxes with major and trace element hydrochemistry and colloidal transport, the study clarifies how hydrology, lithology, and colloidal carriers control carbon and metal transport in one of the largest Arctic river basins.

2. Study Site, Materials and Methods

2.1. Lena River and its tributaries

The Lena River basin has an extremely cold continental climate, with winter air temperatures frequently below −30 °C from December to February. Positive mean air temperatures are generally limited to a thaw period of about five months (May–September). Winter precipitation is low and mostly stored as snow, whereas most annual precipitation occurs in summer, coinciding with peak biological activity and river discharge. Permafrost is predominantly continuous, with discontinuous and sporadic zones in the southern basin (Brown et al., 2002). Along the main stem, mean annual air temperature (MAAT) decreases northward from about −9 °C in the central basin to −13.3 °C in the north, while tributaries span a broader MAAT range from −4.7 to −15.9 °C. Annual precipitation is low, particularly in the northern basin (about 200–250 mm yr^{-1}), but its seasonal maximum occurs in summer. Winter precipitation is smaller and is stored mainly as snow until spring melt (Chevychelov and Bosikov, 2010).

The lithology of the Lena basin upstream of Yakutsk is highly diverse and includes Archean and Proterozoic crystalline and metamorphic rocks, Upper Proterozoic to Ordovician carbonate formations, Permo–Triassic volcanic rocks, and widespread Phanerozoic terrigenous silicate sedimentary units. This geological heterogeneity exerts a major control on riverine major ions, trace elements, and inorganic carbon. More detailed descriptions of basin landscapes, vegetation, and geology are available elsewhere (Rachold et al., 1996; Huh et al., 1999a, b; Huh and Edmond, 1999; Pipko et al., 2010; Semiletov et al., 2011; Kutscher et al., 2017; Ogneva et al., 2023; Juhls et al., 2020, 2025). Together, these climatic, permafrost, and lithological gradients provide the framework for interpreting spatial variability in solute export, greenhouse gas dynamics, and weathering regimes along the Lena River continuum and its tributaries.

2.2. Sampling strategy

In the middle and lower Lena (Yakutsk to Kyusyur), peak annual discharge typically occurs in June and is mainly driven by rapid snowmelt across the permafrost-dominated basin. Sampling was conducted from 5 to 22 July 2022, shortly after peak flow, during the early post-freshet recession. At this stage, river levels remain high but hydrological conditions are more stable than during peak flood, allowing integration of basin-wide snowmelt inputs while reducing short-term variability linked to flood-wave propagation and bank erosion. July conditions also correspond to active-layer deepening and enhanced subsurface connectivity, which promote mobilization of solutes, dissolved inorganic carbon (DIC), dissolved organic carbon (DOC), and greenhouse gases from soils and permafrost-affected terrains.

During the campaign, we navigated ~1500 km aboard the research vessel *Merzlotoved*, from Yakutsk (62.15 °N) to Samoilov Island (72.38 °N) in the Lena Delta (**Fig. 1 A**). A total of 33 sites were sampled along the main stem, together with two major tributaries (Aldan and Vilyui) and four smaller tributaries (Seen-Yurekh, Undyulyung, Bysyttakh, and Molodo). Regular stops at ~50 km intervals along the main channel enabled systematic sampling of major hydrochemical parameters and greenhouse gases (GHG) along the longitudinal river gradient. This transect design aimed to resolve changes in solute composition, dissolved carbon parameters, and CO_2 and CH_4 concentrations in relation to northward permafrost gradients, lithological transitions, and contrasting tributary inputs. At selected confluences, sampling was performed 200–500 m upstream of the mixing zone to obtain representative tributary water and avoid backwater and incomplete mixing effects. Longitudinal transect sampling is widely used to assess river water chemistry in large and climatically extreme basins (Huh and Edmond, 1999; Spence and Telmer, 2005). Sampling during the high-flow season also provides the closest agreement with annual flux estimates derived from time series, because this period accounts for a large share of annual water and solute export (Qin et al., 2006).

2.3. Hydrology and water surface area estimation

July corresponds to the high-flow period of the Lena River, representing the recession phase of the spring freshet (**Fig. 1 B**). Although peak discharge typically occurs in June, river levels remain elevated in July due to delayed snowmelt from northern and high-elevation sub-basins and continued active-layer development in permafrost-dominated terrains. Hydrographs for the studied large rivers were constructed using discharge data from the Automated Information System of the State Monitoring of

Water Bodies (https://gmvo.skniivh.ru/). These time series were used to position the sampling campaign within the seasonal hydrograph and to assess deviations from long-term mean discharge during the sampling period. To characterize hydrological and geomorphological controls on river chemistry, watershed-scale parameters were calculated for each sampling point (**Fig. 1 A**), including total watershed area, river network density, and total watercourse length. These parameters were derived from HydroSHEDS shapefiles (https://www.hydrosheds.org/) using standard GIS procedures.

Water surface area was quantified from Landsat 8–9 Level-2 surface reflectance products (Collection 2) acquired during 5–22 July 2022. Cloud-free scenes were atmospherically corrected, orthorectified, mosaicked, and processed in ArcGIS. Water bodies were delineated using the Normalized Difference Water Index (NDWI) and Modified NDWI (MNDWI), based on green, near-infrared, and shortwave infrared bands, with thresholds calibrated for Lena River conditions, including turbid waters. Classified rasters were converted to polygon shapefiles and manually corrected along shorelines, shallow areas, and zones affected by suspended sediments or aquatic vegetation. In total, 269 water polygons were identified. To improve area accuracy, polygons were subdivided using the Fishnet tool, and surface areas were calculated individually using planar geometry within appropriate WGS 84 / UTM projection zones. Delineation accuracy was visually checked against high-resolution imagery (e.g., Google Earth) and river morphology.

Water discharge at each sampling point and date was estimated from gauging-station data by linear interpolation and hydraulic scaling along the main stem and tributaries, accounting for incremental drainage area and tributary inflows. Surface water discharge, watershed area, river network length, and latitude (used as an integrative proxy of climatic and permafrost gradients) were then compared with surface-water chemistry to assess controls on dissolved major elements, trace elements, and carbon species.

2.4. CO_2 and CH_4 concentrations

Dissolved CO_2 in surface waters was measured in situ using a portable infrared gas analyzer (IRGA; GMT222 CARBOCAP® probe, Vaisala®; accuracy ±1.5%) operating in two ranges (0–2,000 and 0–10,000 ppm). The underway probe was protected by a gas-permeable waterproof PTFE membrane/sleeve. The sensor was installed in the vessel's Kingston water intake system, where continuous flow (~20 L min^{-1}) ensured constant renewal of river water during navigation. A copper mesh was added to reduce potential biofouling (Yoon et al., 2016), although such effects were expected to be minimal in the cold, low-impacted Lena waters.

Independent field checks of water pCO_2 were performed at 24 stations using a second, separately calibrated Vaisala GM70 meter equipped with a GMP222 probe enclosed in an independent gas-permeable PTFE membrane assembly, which allows rapid CO_2 diffusion while preventing water intrusion (Johnson et al., 2009). The control probe was immersed directly at ~20 cm and allowed to stabilize before recording. Temperature and pressure corrections were applied using the same procedure as for the underway sensor. These stationary measurements were used as external checks of the underway record rather than as exact replicate observations, because they were not strictly synchronous or spatially co-located with the Kingston-intake measurements.

At each station, the sensor was equilibrated for ~10 min before measurement. CO_2 concentration (ppm), water temperature (°C), and atmospheric pressure (mbar) were logged every minute using a Campbell data logger during 5-min measurement sequences repeated every 30 min, yielding 153 individual records. For the main stem, values were averaged over three consecutive 5-min sequences. At tributary confluences, measurements were performed 200–500 m upstream of the mixing zone. Sensors were calibrated before and after the expedition against certified gas standards (0, 800, 3,000, and 8,000 ppm), yielding linear relationships with $R^2 > 0.99$. Instrumental drift ranged from 0.03 to 0.06% d^{-1}, and post-processing corrections for temperature and pressure followed Johnson et al. (2009). Overall uncertainty of individual pCO_2 measurements was ≤10%.

Methane concentrations were determined from unfiltered water collected in 60 mL serum bottles without headspace, preserved with 0.2 mL saturated $HgCl_2$, and analyzed in the laboratory by headspace equilibration with ultra-high-purity N_2. Two 0.5 mL aliquots of the equilibrated headspace were measured on a Bruker GC-456 gas chromatograph equipped with flame ionization and thermal conductivity detectors. Calibration was performed every 10 samples using certified standards (Air

Liquide; 145 ppmv), and duplicate injections showed reproducibility within ±5%. Dissolved CH_4 concentrations were calculated from headspace measurements using temperature-dependent solubility coefficients (Yamamoto et al., 1976) and mass-balance equations. Combined uncertainty of CH_4 concentrations was estimated at 7–12%. These analytical uncertainties are small relative to the observed spatial gradients in CO_2 and CH_4 and do not affect the interpretation of longitudinal and tributary-scale patterns.

2.5. Flux measurement and calculation

Diffusive CO_2 fluxes (F_{CO_2}) were measured using two floating chambers (ca. 30 cm diameter, ~10 L volume) equipped with non-dispersive infrared CO_2 sensors (SenseAir). Sensors were calibrated in the laboratory against certified N_2–CO_2 gas mixtures prior to field deployment. During measurements, chambers floated freely at the water surface, and headspace CO_2 was recorded over 5-min intervals. Fluxes were calculated from the initial linear accumulation phase using the first 30 min of deployment (Serikova et al., 2018; Vorobyev et al., 2024).

In addition to direct chamber measurements, diffusive CO_2 fluxes were independently estimated using the bulk gas exchange equation of Cai and Wang (1998):

$$F_{CO_2} = K_h\, k_{CO_2}\, (C_{water} - C_{air})\,, \qquad (1)$$

where K_h is the Henry's constant corrected for temperature and pressure (mol L^{-1} atm^{-1}), k_{CO_2} is the gas exchange velocity at a given temperature, C_{water} is the water CO_2 concentration, and C_{air} is the CO_2 concentration in the ambient air. Conversion between dissolved concentration and partial pressure followed Wanninkhof et al. (1992) and Lauerwald et al. (2015). Atmospheric CO_2 for July 2022 was taken as 417.9 ppm from the WMO global monitoring network, consistent with the nearest Tiksi station (422.5 ppm; https://community.wmo.int/wmo-greenhouse-gas-bulletins; https://www.meteorf.gov.ru/product/infomaterials/90/). Temperature-dependent solubility constants followed Wanninkhof et al. (1992).

A median gas transfer velocity of 4.46 m d^{-1} was adopted from measurements in four major Western Siberian rivers (Karlsson et al., 2021), consistent with previous estimates for the Lena River (Vorobyev et al., 2021a), the Kolyma (Denfeld et al., 2013), the Yukon (Striegl et al., 2012), and global syntheses for large rivers (Alin et al., 2011; Raymond et al., 2013). Wind speeds during sampling were below 3.7 m s^{-1} and water surfaces were visually smooth, supporting the use of this literature-constrained K_T value (Jähne et al., 1987; Alin et al., 2011; Guérin et al., 2007).

Instantaneous diffusive CH_4 fluxes were calculated using an equation analogous to Eq. (1), with gas transfer velocities derived from chamber-measured CO_2 fluxes and in situ CO_2 concentrations, following approaches used for Western Siberian rivers (Serikova et al., 2018; Lim et al., 2022; Vorobyev et al., 2024). Dissolved CH_4 concentrations were combined with atmospheric equilibrium concentrations assuming a background atmospheric pCH_4 of 1.8 ppm and the 2022 mean atmospheric CH_4 concentration from Mauna Loa Observatory (http://aftp.cmdl.noaa.gov/products/trends/ch4/ch4_annmean_gl.txt), following Serikova et al. (2018, 2019). Flux uncertainty was dominated by variability in gas transfer velocity rather than by analytical uncertainty in dissolved gas concentrations. Concentration uncertainty contributed comparatively little (≤10% for CO_2 and 7–12% for CH_4), whereas k_{CO_2} may vary by ±40–60% depending on hydraulic conditions (Raymond et al., 2013). Sensitivity analysis showed that using a conservative k_{CO_2} value of 3 m d^{-1} instead of 4.46 m d^{-1} would decrease calculated CO_2 emissions by about 30%, while preserving the spatial patterns along the transect. Because the objective of this study is to resolve relative gradients between tributaries and main stem sections rather than derive absolute annual budgets, the adopted k_{CO_2} parameterization provides a robust and internally consistent basis for comparative flux analysis.

2.6. *Physicochemical parameters and laboratory analyses*

In situ dissolved oxygen, specific conductivity, and water temperature were measured at ~20 cm depth using a WTW 3320 multimeter equipped with a CellOx 325 oxygen probe (±5%), a TetraCon 325 conductivity sensor (±1.5%), and a temperature sensor (±0.2 °C). pH was measured with a portable

Hanna instrument fitted with a combined Schott glass electrode, calibrated daily with NIST-traceable buffers (pH 4.01, 6.86, and 9.18 at 25 °C), yielding an uncertainty of ±0.01 pH units. Buffer temperatures were kept within ±5 °C of river water temperature.

Surface water was collected from 20–30 cm depth near the channel center into pre-cleaned polypropylene bottles and immediately filtered through sterile single-use Sartorius filters (0.45 µm). The first 50 mL of filtrate were discarded. Milli-Q blanks confirmed negligible DOC contamination from the filters. Filtered samples were split into aliquots: one was acidified to 2% (v/v) with bidistilled HNO_3 in pre-cleaned polypropylene vials for major and trace element analyses; the second, non-acidified fraction was used for DOC, DIC, and UV absorbance. Samples were stored at 4 °C and analyzed within 30 days.

DOC and DIC were measured with a Shimadzu TOC-VSCN analyzer (detection limit 0.1 mg L^{-1}; precision ±3%). Nutrients were analyzed on frozen filtered samples by ion chromatography (Dionex ICS-5000+) with ±2% uncertainty; certified reference materials Ion-915 and Ion-964 were within 10% of certified values. Total bacterial cell concentration (TBC) was measured by flow cytometry after fixation with glutaraldehyde, following Marie et al. (1999). Major and trace elements were determined in acidified samples by ICP-MS (Agilent 7500ce, Ar and He modes). Precision ranged from 5–10% at 1–1000 µg L^{-1} to 10–20% at 0.001–0.1 µg L^{-1}. Accuracy and reproducibility were checked using SLRS-6 (River Water Certified Reference Material for Trace Metals and other Constituents, Canada) and three in-house multi-element standards every 20 samples (Yeghicheyan et al., 2019), with agreement within 10–15% for 40 elements.

Twelve selected samples were additionally processed by dialysis (1 kDa cutoff) to distinguish low-molecular-weight (<1 kDa) and colloidal (1 kDa–0.45 µm) fractions. River water was pre-screened through a 20 µm nylon mesh and placed in cleaned 5 L polyethylene containers; pre-cleaned 50 mL dialysis bags were immersed for 3–5 days following established procedures (Vasyukova et al., 2010; Pokrovsky et al., 2016b; Kolesnichenko et al., 2021). Containers were kept dark at near in situ temperature and gently agitated. Dissolved solute concentrations before and after dialysis differed by <10% ($p > 0.05$), indicating negligible alteration of dissolved and colloidal composition during incubation. Nevertheless, dialysis provides operational rather than structural size separation. During the

3-5 day equilibration, some redistribution among colloidal subfractions, aggregation/disaggregation, adsorption/desorption on container or membrane surfaces, and limited microbial alteration cannot be fully excluded. Therefore, the 1 kDa–0.45 µm fraction is interpreted here as an operational colloidal pool, and not as an indicator of the exact in situ colloidal size spectrum.

2.7. Statistical treatment of the data

Pearson correlations were calculated to assess linear relationships between variables, and statistical significance was evaluated at $p < 0.05$. To further identify the dominant drivers of dissolved carbon variability (CO_2, DIC, and DOC), multivariate statistical analysis was performed using Principal Component Analysis (PCA). This approach allowed us to assess the combined influence of hydrochemical parameters (major ions, nutrients, trace elements), hydrological variables (discharge, watershed area), and climatic factors (e.g., latitude as an integrative proxy) on spatial patterns of dissolved carbon in river waters. The analysis was performed using STATISTICA 7 (StatSoft Inc., http://www.statsoft.com). Principal components were extracted from the raw data matrix using the covariance structure of standardized variables.

PCA was performed on the correlation matrix of standardized variables. Given the limited number of main stem samples ($n = 26$), the large number of hydrochemical variables, and the modest cumulative variance represented by the first two axes, PCA was used only as an exploratory ordination. The number of components was evaluated using the scree plot. The first two Varimax-rotated components, explaining 23% and 13% of total variance, respectively (36% cumulative), were retained to visualize the clearest covariance structure. Interpretations were accepted only when consistent with pairwise correlations and independent size-fractionation evidence; no causal or discrete cluster assignment was inferred from PCA alone. PCA was therefore used as an exploratory tool to identify major axes of covariation, rather than as a complete explanation of hydrochemical variability.

3. Results

3.1. Hydrological parameters

Hydrograph analysis (**Fig. 1 B**) indicates that river discharge during the study period was primarily sustained by groundwater contributions and rainfall inputs following the spring snowmelt peak. By July, the Lena River was in the recession phase of the freshet, characterized by gradually declining but still elevated discharge likely sustained by delayed runoff, rainfall, and subsurface contributions. The estimated water travel time between the upstream gauging station at Tabaga and the downstream station at Kyusur was approximately 12 days under the observed hydrological conditions. This relatively short transit time implies efficient downstream propagation of water masses and associated solutes along the main stem during high-flow conditions.

The drainage network of the Lena basin is well developed, with a mean river network density of 0.22 km km^{-2}. According to Strahler's classification, stream order within the basin ranges from first-order headwater streams to ninth-order channels along the main stem, reflecting the hierarchical organization and large spatial integration of tributary inputs. Hydrologically, 2022 corresponded to a relatively high-flow year when compared to long-term records prior to the 1970s. Mean annual discharge reached 10,501 m^3 s^{-1} at Tabaga and 19,745 m^3 s^{-1} at Kyusur, placing 2022 among the upper range of historical values. However, in the context of the past two decades, these values fall within the range of average annual discharge reported by the Russian Federal Service for Hydrometeorology and Environmental Monitoring (Roshydromet), consistent with recent assessments (Juhls et al., 2025). Thus, while elevated relative to early historical records, hydrological conditions during the expedition were representative of contemporary flow regimes in the Lena River. The combination of high discharge, rapid downstream water transit (~12 days), and strong tributary integration created conditions favorable for efficient longitudinal transport of dissolved carbon species and greenhouse gases, setting the framework for interpreting spatial gradients in CO_2, CH_4, DIC, DOC, and associated emission fluxes.

3.2. Dissolved carbon species and greenhouse gases along the Lena continuum

Under the elevated but hydrologically representative discharge conditions of July 2022, the Lena River system provides an opportunity to evaluate how basin-wide connectivity, tributary integration, and northward climatic gradients regulate dissolved carbon pools and greenhouse gas dynamics. Below, we describe the spatial distribution of pCO_2, CH_4, DIC, and DOC along the main stem and tributaries, and quantify associated diffusive carbon fluxes.

The principal hydrochemical carbon parameters of the Lena River main stem (pCO_2, CH_4, pH, O_2, E.C., DIC, and DOC) are summarized in **Table 1**. Along the main stem, DIC showed a weak, statistically non-significant northward increase, whereas DOC showed no systematic longitudinal trend **(Fig. 2 A, B)**. Mean concentrations were 8.4 ± 2.7 mg L^{-1} for DIC and 7.5 ± 2.7 mg L^{-1} for DOC. Discrete pCO_2 measurements indicated a weak northward decrease, with a mean value of 1020 ± 420 µatm (median 892 µatm; range 600–2600 µatm; **Fig. 2 C**). Chamber-derived CO_2 fluxes ranged from 0.11 to 0.82 g C–CO_2 m^{-2} d^{-1} along the main stem (**Fig. 2 D**), whereas calculated fluxes across the main stem and tributaries ranged from near-zero values to 1.3 g C m^{-2} d^{-1}. Methane concentrations were low (mean 0.22 µmol L^{-1}; median 0.08 µmol L^{-1}) and showed no significant longitudinal trend (**Fig. 2 E**). Diffusive CH_4 emissions contributed <0.5% of total carbon emissions (**Fig. 2 F**).

When continuous pCO_2 measurements along the main stem (153 individual data points, with mean distance of 7.25 km) are examined along the south–north transect together with discrete observations from tributaries (**Fig. 3 A**), major tributary confluences emerge as clear discontinuities in the longitudinal pattern. These zones are characterized by abrupt increases or decreases in CO_2 concentration, reflecting the input of waters with contrasting biogeochemical signatures. The independent control measurements reproduced the broad magnitude and spatial pattern of the underway pCO_2 record but showed larger pointwise differences at several stations. These divergences occurred mainly across steep pCO_2 gradients and close to tributary confluences. Underway values represent moving averages over ~1.25-km river segments, whereas the controls are stationary snapshots; differences can therefore reflect short-distance or cross-channel heterogeneity, incomplete tributary mixing, small depth offsets, and the different equilibration response of the two membrane assemblies.

Because the controls showed no consistent directional offset, the mismatches were not interpreted as evidence of systematic sensor bias.

A similar pattern is observed for calculated continuous CO_2 fluxes (**Fig. 3 B**). The Vilyui River exhibited the highest emissions (up to 1.3 g C–CO_2 m^{-2} d^{-1}), highlighting its role as a major localized source of CO_2 to the main stem. In contrast, the Aldan chamber measurement was close to zero, whereas pCO_2 indicated supersaturation and a small positive calculated flux during the sampling period, indicating substantial spatial variability in tributary influence. Despite this pronounced local heterogeneity, the main stem displayed relatively stable dissolved carbon characteristics. DOC concentrations remained spatially uniform, and DIC showed only a weak longitudinal trend, whereas pCO_2 and FCO_2 exhibited dynamic variability controlled by tributary inputs and in-stream processes. As a result, the Lena River evaded CO_2 to the atmosphere during July 2022. In contrast, CH_4 concentrations were low and varied non-systematically, contributing only marginally to total carbon emissions. This pattern further supports the decoupling between bulk dissolved carbon pools and CO_2 evasion, with tributaries acting as primary factors of short-scale variability along the river continuum, as was also evidenced in earlier study of upper and middle Lena reaches (Vorobyev et al., 2021a).

3.3. Areal emission from the Lower Lena River basin

Previous estimates of areal CO_2 emissions from lotic waters of the Lena River basin were based on total river surface coverage for the entire watershed, estimated at 28,197 km^2 in 2016, including 5,022 km^2 of seasonal water (Global SDG database; Vorobyev et al., 2021a). This value is broadly consistent with the Global River Widths from Landsat (GRWL) Mask estimate of 22,479 km^2. In contrast, the present calculation was restricted to the Lower Lena sector between Yakutsk and Kyusyur, covering 1,551,445 km^2 of land area and 12,904 km^2 of water surface. This included the main stem (7529 km^2) and the two largest tributaries, the Aldan and Vilyui Rivers, with water surface areas of 2377 and 2998 km^2, respectively.

The emission estimate corresponds to the hydrological conditions of the expedition, i.e. the transition from the end of the spring flood to the onset of summer baseflow. This sector was previously identified as a major source of uncertainty for Lena River emission estimates because of the lack of direct pCO_2 and flux measurements downstream of the Aldan confluence and across the Vilyui-influenced reach. During July 2022, the Aldan River showed near-zero chamber-measured CO_2 exchange (FCO_2 = –0.03 μmol m^{-2} s^{-1}; pCO_2 = 1014 μatm), whereas the Vilyui River exhibited the highest chamber-derived emission measured during the campaign (1.3 g C m^{-2} d^{-1}; pCO_2 = 1340 μatm). Fluxes calculated from pCO_2 for these two tributaries were more similar, amounting to 0.31 and 0.485 g C m^{-2} d^{-1} for the Aldan and Vilyui, respectively.

For the main stem, the chamber-derived mean CO_2 flux was 0.33 ± 0.20 g C m^{-2} d^{-1} (n = 12) along the south–north transect. Fluxes calculated from continuous and discrete pCO_2 measurements (mean 957 ± 230 μatm, n = 153) using (K_T = 4.46) m d^{-1} yielded nearly identical values of 0.32 ± 0.20 g C m^{-2} d^{-1} (**Fig. 2 C, D;** Fig. 3). The experimentally derived piston velocity calculated from paired chamber fluxes and pCO_2 measurements averaged (K_T = 8.82 ± 6.76) m d^{-1}, indicating substantial spatial variability in gas exchange conditions. However, the close agreement between chamber-derived and pCO_2-derived mean fluxes supports the use of (K_T = 4.46) m d^{-1} for reach-scale comparative upscaling. Emission estimates were then weighted according to the relative water surface areas of the main stem (58% of the total Lower Lena water area), Vilyui (23%), and Aldan (18%). The resulting water-area-weighted CO_2 emission estimate for the Lower Lena during the transition from the end of spring flood to early baseflow was 0.36 ± 0.15 g C m^{-2} d^{-1}.

3.4. Spatial pattern of major and trace solutes

All measured hydrochemical parameters for the Lower Lena River and its tributaries are reported in Table S1 (Supplementary Excel file). Based on longitudinal trends along the main stem, three principal groups of solutes were identified: (*i*) Low-solubility trivalent and tetravalent elements and strong hydrolysates, exhibiting a significant northward decrease in concentration (**Fig. 4**). This group includes Al, Sc, Ga, Y, rare earth elements (REEs), Ti, Th, U, Be, and Nb. These elements are typically associated with particulate or colloidal phases and exhibit systematic downstream decline along the river continuum. (*ii*) Labile major cations and anions (including host carbonate mineral-related solutes), showing increasing concentrations from south to north (**Fig. 5**). This group comprises DIC, SO_4^{2-}, B, Mg, P, Ca, Sr, As, Se, and Sb, consistent with progressive downstream integration of groundwater inputs and deep bedrock/weathering inputs. Third group includes components without statistically significant longitudinal trends, defined by correlation coefficients $|r| < 0.3$ ($p > 0.05$) with latitude (**Table S2**). This category includes DOC, greenhouse gases (CO_2 and CH_4), major anions (Cl^-, F^-, NO_3^-), Si, K, V, Cr, Mn, Fe, Ni, Cu, Zn, Co, Cd, Rb, Mo, Cs, Ba, Hf, W, Tl, Pb, and Bi. These solutes exhibited spatial variability but no systematic south–north gradient along the main channel.

In addition to longitudinal patterns, distinct local anomalies were observed in certain tributaries. For example, Mn concentrations in the Undyulyung River (LIV 17) exceeded adjacent main stem values by a factor of 27. Similarly, Fe and Mn concentrations in the Bysyttakh and Molodo tributaries (LIV 28 and LIV 29) were elevated relative to the main channel by factors of approximately 2 and 5, respectively. However, such deviations were not widespread. For most elements, concentrations in tributaries were comparable to those measured in neighboring main stem sections, typically within ±30% of adjacent values. This overall similarity indicates efficient mixing and strong integration of tributary inputs within the large-channel hydrodynamic framework of the Lower Lena.

3.5. Correlations and multiparametric treatment

Multivariate statistical treatment was restricted to the Lena main stem ($n = 26$), as the number of sampled tributaries ($n = 6$) was insufficient for robust statistical analysis. Pairwise Pearson correlation analysis revealed several significant relationships among dissolved constituents ($p < 0.05$; **Table S2**). pCO_2 correlated positively with F^-, Cl^-, and Na^+. Diffusive CO_2 flux correlated positively with DOC ($r = 0.87$, $p < 0.01$; **Fig. 6 A**), nutrients (P, K), and selected trace metals (V, Ni). In contrast, CH_4 concentrations did not show significant correlations with the measured hydrochemical parameters. DIC correlated positively with Br^-, Si, P, Rb, and As, as illustrated by the DIC–As relationship in **Fig. 6 B**. Aluminum showed strong positive correlations with Ti, Ga, Y, and REEs (**Fig. 6 C, D**), and weaker positive correlations with Th and U.

Principal Component Analysis (PCA) was applied to the standardized main-stem dataset. The first two Varimax-rotated components explained 23% and 13% of total variance, respectively (36% cumulative; **Fig. 7; Table S3**). Along rotated component 1, positive loadings of Be, Al, Ti, Ga, Y, Nb, REEs, and Th contrasted with negative loadings of B, SO_4^{2-}, DIC, Mg, and Sr. Rotated component 2 grouped DOC with P, K, V, Mo, Co, Ni, As, Sb, and Cs, whereas latitude showed only moderate loading. Thus, PCA summarized the main covariance structure of the dataset but did not account for most of the total variance. These correlation and PCA patterns provide the statistical basis for the operational size-fractionation analysis as presented in the next section.

3.6. Colloidal Status of Major and Trace Elements in the Lena River and Tributaries

Dialysis (1 kDa cutoff) enabled operational separation of nominal low-molecular-weight ($LMW_{<1\ kDa}$) and dissolved (< 0.45 µm) colloids with sizes > 1 kDa. The colloidal proportion of each element *i* was calculated as the percentage of its concentration in the 1 kDa–0.45 µm fraction relative to its concentration in the dissolved (< 0.45 µm) form following:

$$[i]_{colloidal} = 100\% \times ([i]_{0.45\ \mu m} - [i]_{<1\ kDa}) / [i]_{0.45\ \mu m}$$

where $[i]_{<0.45\ \mu m}$ and $[i]_{<1\ kDa}$ are concentrations of element in the 0.45 µm filtrate and 1 kDa dialysate, respectively.

Across the northern Lena basin, the relative contribution of colloidal forms was remarkably consistent between the main stem and tributaries (**Fig. 8**). The colloidal fraction ranged from negligible values (0–10%) for highly soluble species such as DIC, Li, and Si, to dominant proportions (80–90%) for trivalent and tetravalent hydrolysates. Based on colloidal abundance, three principal groups of solutes were distinguished: (1) Predominantly truly dissolved species (0–20% colloidal fraction): Alkali and alkaline-earth metals (Li, Na, K, Rb, Mg, Ca, Sr), major inorganic carbon (DIC), Si, and selected trace oxyanions (Mo, As). These elements were largely present in low-molecular-weight forms and exhibited minimal association with colloidal phases. (2) Mixed LMW–colloidal species (20–60% colloidal fraction): P, Al, and several trace metals (Cu, V, Sc, Ni, Cr, Co, U) showed intermediate colloidal contributions. Dissolved organic carbon (DOC) exhibited a mean colloidal proportion of 41 ± 14%, indicating that a substantial fraction of riverine organic matter was associated with supramolecular or organo-mineral colloidal structures. Here, colloidal DOC refers operationally to the organic-carbon fraction retained between 1 kDa and 0.45 µm. This fraction should not be interpreted as a single physical class of particles, but as a continuum of humic supramolecular associations, high-molecular-weight organic macromolecules, microbial and plant-derived polymers, and organic coatings or complexes associated with Fe- and Al-rich mineral phases. The last, 3rd group of solutes, included predominantly colloidal elements (80–90% colloidal fraction) such as certain divalent metals (Mn, Ba, Zn, Pb) and refractory lithogenic hydrolysates (Fe, Ga, Y, REEs, Ti, Zr, Hf, Th, Be, Nb). These were largely transported in colloidal form, consistent with strong hydrolysis tendencies and association with Fe-rich mineral or organo-mineral particles. No major difference in colloidal partitioning was observed between the main stem and tributaries. In particular, DOC exhibited a remarkably uniform colloidal proportion (41 ± 14%) across the main stem and four tributaries, including the largest ones (Vilyui and Aldan). The only notable deviation occurred in a floodplain lake hydrologically disconnected from the main channel, where DOC, Al, and Co displayed 20–30% higher colloidal fractions relative to fluvial waters. Overall, the Lena River system exhibited a highly structured and spatially homogeneous colloidal pattern, with refractory lithogenic elements transported predominantly in colloidal form, mobile weathering-derived solutes remaining largely truly dissolved, and DOC having an intermediate and remarkably stable colloidal proportion across the basin.

4. DISCUSSION

The Lower Lena River during the post-freshet high-flow period exhibited spatially distinct but internally consistent hydro-biogeochemical organization. While bulk dissolved carbon pools (DOC and DIC) remained relatively stable along the main stem, CO_2 was systematically supersaturated, sustaining moderate but spatially variable atmospheric evasion. In parallel, major and trace solutes demonstrated clear longitudinal patterns: weathering-derived labile solutes progressively increased downstream, low-solubility lithogenic hydrolysates declined, and the majority of redox-sensitive and nutrient elements showed no systematic gradient. Multivariate statistics and size-fractionation analyses further demonstrated that this pattern likely stems from interplay of groundwater connectivity, lithological control, and colloidal transport, which together regulate both dissolved carbon dynamics and trace-element mobility. Below, we place these observations into the broader context of Arctic river biogeochemistry and evaluate specific mechanisms controlling solute and greenhouse gas transport in the Lower Lena basin.

4.1. Carbon pools, gas exchange, and areal CO_2 emissions in the Lower Lena

4.1.1. Carbon pools and greenhouse gases in the context of previous Lena observations

Bulk DOC and DIC concentrations measured during this campaign were within the range previously reported for the Lena during summer and late-summer conditions. DOC values were consistent with earlier range of 2 to 12 mg L^{-1}, whereas DIC concentrations were close to reported summer values of about 10 mg L^{-1} (Cauwet and Sidorov, 1996; Lara et al., 1998; Lobbes et al., 2000; Kuzmin et al., 2009; Kutscher et al., 2017; Sun et al., 2018; Juhls et al., 2020, 2025; Semiletov et al., 2011). In contrast, pCO_2 values in July 2022 were higher than previous late-summer estimates from the lower Lena (Semiletov, 1999; Semiletov et al., 2011; Pipko et al., 2010), suggesting that the post-freshet recession still retained stronger CO_2 supersaturation than later-season baseflow. Methane concentrations were low and comparable to earlier measurements from the upper, middle, and lower Lena (Bussmann, 2013; Vorobyev et al., 2021a), confirming the subordinate role of CH_4 in open-channel C emissions during this hydrological period.

4.1.2. Choice of flux values for upscaling and comparison with previous emission estimates

For the areal emission estimate, we focused on the Lower Lena sector rather than the entire Lena basin. Previous basin-wide assessments used total river-water coverage of 28,197 km² from the Global SDG database, broadly consistent with the 22,479 km² river surface area from the GRWL Mask database. Here, Landsat-based delineation constrained the studied Lower Lena water surface to 12,904 km², including the main stem, Aldan, and Vilyui. This distinction is important because the present estimate represents the post-freshet Lower Lena reach rather than a whole-basin annual emission budget.

The choice of flux value for upscaling was constrained by agreement between independent approaches. The chamber-derived main-stem flux averaged 0.33 ± 0.20 g C m^{-2} d^{-1}, while fluxes calculated from continuous/discrete pCO_2 (using K_T = 4.46 m d^{-1}) yielded nearly identical values of 0.32 ± 0.20 g C m^{-2} d^{-1}. Although paired chamber and pCO_2 measurements produced a higher and variable apparent piston velocity (K_T = 8.82 ± 6.76 m d^{-1}), the agreement between measured and calculated fluxes supports the use of K_T = 4 to 4.5 m d^{-1} for comparative upscaling. This value is consistent with gas-transfer velocities used for large Siberian rivers and global river syntheses (Raymond et al., 2013; Karlsson et al., 2021; Vorobyev et al., 2021a, 2024).

The resulting water-area-weighted CO_2 emission from the Lower Lena was 0.36 ± 0.15 g C m^{-2} d^{-1}. This is lower than the 1.65 ± 0.5 g C m^{-2} d^{-1} previously reported for the upper and middle Lena during peak freshet (Vorobyev et al., 2021a). The difference likely reflects both seasonal and spatial contrasts: peak snowmelt promotes flushing of CO_2-rich soil and shallow subsurface waters, whereas post-freshet recession reduces lateral CO_2 supply and allows continued degassing and greater in-stream primary production (Pipko et al., 2010; Semiletov et al., 2011; Juhls et al., 2020, 2025; Krickov et al., 2023). Because the two estimates derive from different expeditions and different river sectors, this comparison should be interpreted as a plausible seasonal contrast rather than a paired temporal assessment.

The chamber-derived CO_2 emissions measured along the Lower Lena main stem were within the lower range of values previously reported for large Arctic and boreal rivers such as the Ob River main channel in permafrost-free regions (1.32 ± 0.14 g C m^{-2} d^{-1}; Karlsson et al., 2021), small rivers within the continuous permafrost zone of western Siberia (0.98 g C m^{-2} d^{-1}; Serikova et al., 2018), and the Low Ob River during spring flood peak (1.56 ± 0.47 g C–CO_2 m^{-2} d^{-1}; Vorobyev et al., 2024). At the same time, Lena's fluxes are very similar to those of the Kolyma River main stem (0.35 g C m^{-2} d^{-1}; Denfeld et al., 2013). Thus, under post-freshet summer conditions, the Lower Lena behaves as a moderate but persistent CO_2 source to the atmosphere, consistent with the broader Arctic riverine carbon paradigm.

4.1.3. Tributary control, CH_4, and DOC/DIC–pCO_2 decoupling

As previously documented for the upper and middle Lena during peak spring discharge (Vorobyev et al., 2021a), pCO_2 along the main stem exhibited marked short-distance variability (**Fig. 3 A**), reflecting the interplay of external inputs and in-stream processing. Tributary inflows with contrasting CO_2 signatures are widely recognized as primary drivers of spatial heterogeneity in Arctic river systems (Crawford et al., 2013; Leith et al., 2014, 2015; Hotchkiss et al., 2015; Dean et al., 2020; Vonk et al., 2023). In addition to this lateral variability, internal riverine processes—including turbulence-controlled gas exchange (Raymond et al., 2013; Rocher-Ros et al., 2023), sediment resuspension and benthic respiration (Hopkinson, 1985; Humborg et al., 2010), and mineralization of organic carbon in the water column (Cole et al., 2007; Attermeyer et al., 2018)—can modify CO_2 concentrations over short spatial scales. Furthermore, in permafrost-dominated catchments, there is substantial lateral inflow of CO_2-rich suprapermafrost waters derived from thawed active layers and shallow groundwater pathways (Bagard et al., 2011; Vonk et al., 2015; Raudina et al., 2018; Vorobyev et al., 2024; Krickov et al., 2026). Given that our measurements were averaged over ~1.5 km segments, the observed fluctuations cannot be attributed to analytical noise but instead reflect real spatial heterogeneity in CO_2 dynamics along the main channel.

The uniformly low CH_4 concentrations probably reflected the hydrological state of the river during the post-freshet recession. By July, connectivity with shallow floodplain ponds, wetlands, and anoxic inundated soils was likely reduced relative to peak flood, limiting inputs from strongly methanogenic environments (Sachs et al., 2008; Bastviken et al., 2011; Stanley et al., 2016). At the same time, the well-oxygenated main channel favored methane oxidation and rapid turbulent exchange, whereas deep and fast-flowing sections likely had limited interaction with anoxic sediments and floodplain sources (Stanley et al., 2016; Bussmann et al., 2017; Rocher-Ros et al., 2023). The single floodplain lake sample, which showed elevated CH_4 together with high pCO_2, supports the view that hydrologically disconnected or weakly flushed floodplain waters can act as localized methane-rich environments, whereas the main stem remains a weak CH_4 source (Bussmann, 2013; Serikova et al., 2019).

Among all dissolved carbon variables, only pCO_2 displayed a statistically significant latitudinal pattern, decreasing from south to north. This gradient likely reflects a combination of multiple factors. First, southern reaches receive substantial contributions from the Aldan and Vilyui tributaries, whose watersheds encompass extensive forested and more productive landscapes, promoting higher terrestrial CO_2 inputs. Second, vegetation density and soil organic carbon stocks generally decline northward, potentially reducing lateral CO_2 supply from soils. Third, progressive hydrological disconnection between soil water and the river network toward the delta, together with increased channel width and reduced turbulence, may enhance degassing efficiency and decrease downstream pCO_2. Collectively, these factors suggest that the south-to-north decline in pCO_2 integrates shifts in terrestrial carbon supply, tributary influence, and hydrodynamic processing along the Lower Lena continuum. The modest downstream cooling of river water, from approximately 18 to 15–16 °C, may have slightly reduced microbial and abiotic CO_2 production, but this effect was likely secondary relative to tributary inputs, lateral carbon supply, and hydrodynamic degassing.

A notable result is that pCO_2 was decoupled from bulk DOC and DIC concentrations. Indeed, during the sampled period, neither DOC nor DIC showed a significant trend ($R^2 < 0.18$) with latitude, whereas pCO_2 declined northward ($R^2 > 0.52$) and varied markedly over short distances. This concentration-level decoupling indicates that CO_2 supersaturation was controlled more by production, lateral inputs, and evasion than by the size of the bulk dissolved-carbon pools. In large Arctic rivers, DIC integrates carbonate weathering, groundwater inputs, and in-stream transformations, whereas pCO_2 responds rapidly to respiration, suprapermafrost inflows, pH, and hydrodynamic degassing (Mu et al., 2025; Zhang et al., 2026). Comparable behavior has been reported in other high-latitude rivers, where rapid lateral exchange and gas loss coexist with relatively modest variability in DOC and DIC concentrations (Crawford et al., 2013; Karlsson et al., 2021; Vorobyev et al., 2024). Stable bulk concentrations, however, do not imply invariant composition or reactivity. Previous Lena studies documented seasonal and longitudinal changes in DOM sources and optical properties despite modest concentration changes (Amon et al., 2012; Kutscher et al., 2017; Juhls et al., 2020; Pipko et al., 2023), whereas our dataset cannot resolve DOC molecular composition, biodegradability, photoreactivity, or residence time. DIC is likewise a composite pool: at pH 6.78–7.70, bicarbonate is expected to dominate, while dissolved CO_2* remains highly responsive to respiration, groundwater inputs, pH, and air–water exchange (Pipko et al., 2010; Semiletov et al., 2011). Thus, relatively stable total DIC can coexist with pronounced pCO_2 variability, and the DOC–FCO_2 relationship should be interpreted as covariance rather than demonstrated causation. In summary, bulk DOC and DIC concentrations were comparatively uniform, whereas pCO_2 varied locally and declined northward, indicating stronger control by hydrological connectivity and gas exchange than by dissolved-carbon stocks. The next section places these carbon patterns within the broader framework of major- and trace-solute transport in the Lower Lena.

4.2. Major and trace solute transport: long-term consistency, colloidal carriers, and multivariate support

4.2.1. Long-term consistency of major solutes and comparison with recent spatial surveys

Several datasets documented major solute concentrations in the Lena main stem during summer baseflow. The concentrations of major solutes measured in the present study (Na, Cl, Si, Ca, Mg, SO_4, DIC) agree within 30% with values reported for the Yakutsk–Kyusyur sector during July–August (Kuzmin et al., 2009; Juhls et al., 2020). Similarly, comparison with long-term hydrochemical monitoring at the Kyusur gauging station (Gordeev and Sidorov, 1993), as well as more recent datasets from the PARTNERS and ARCTIC GRO programs (Cooper et al., 2008; Holmes et al., 2012; McClelland et al., 2015; Gordeev et al., 2024) and high-frequency sampling at Samoylov Island (Opfergelt et al., 2024; Juhls et al., 2025), demonstrates agreement within 20–30% for Si, SO_4, Cl, F, Ca, K, Mg, Na, Al, Mn, and Sr at the northernmost sampling points. Fe concentrations measured here were approximately two times higher, whereas NO_3 concentrations were up to six times lower than previously reported. These deviations reflect local redox conditions, biological uptake, and space- and seasons-dependent partitioning of Fe between colloidal and particulate phases (Hirst et al., 2020).

The most spatially extensive recent surveys of the lower Lena north of Yakutsk were conducted by Swedish research teams (Murphy et al., 2018; Sun et al., 2018; Hirst et al., 2017, 2020; Mavromatis et al., 2024). Dissolved concentrations of Li, Na, K, Mg, Si, Al, and Fe measured in this study fall within the ranges reported for July–August conditions by these authors. This agreement across independent expeditions underscores the reproducibility of Lena hydrochemistry during the open-water season and suggests that contemporary climatic warming has not yet induced drastic shifts in bulk solute export during summer baseflow. Variability in most solutes rarely exceeded a factor of 2–3, reinforcing the view that the Lower Lena behaves as a chemically stable system during this period. Overall, the consistency across datasets spanning more than five decades and ~1500 km of the main stem indicates remarkable temporal and spatial stability of major solute concentrations during summer baseflow conditions. Such stability is characteristic of large Arctic rivers where deep groundwater inputs and basin-scale integration of surface fluxes reduce short-term variability.

4.2.2. Colloidal carriers and trace element mobility

The longitudinal solute groups identified in the Results can be interpreted as the outcome of two contrasting transport modes. The northward increase in DIC, Ca, Mg, Sr, SO_4^{2-} and related mobile species points to increasing influence of groundwater connectivity and water–rock interaction, whereas the northward decline of Al, Ti, REEs, Th, U and other hydrolysates indicates dilution, sedimentation, or colloidal removal of low-solubility lithogenic components. Local Fe–Mn enrichments in several tributaries likely represent specific redox-sensitive end members rather than a basin-scale gradient.

Dissolved organic matter and DOM-stabilized Fe and Al oxyhydroxides are widely recognized as dominant colloidal carriers of trace elements in boreal and permafrost-affected humic waters (Loiko et al., 2017; Raudina et al., 2021; Stolpe et al., 2013a,b; Cuss et al., 2017, 2018, 2020; Vasyukova et al., 2010; Ilina et al., 2014, 2016). Although based on a limited number of dialysis samples, our operational size-fractionation results support that dissolved (<0.45 µm) low-solubility trivalent and tetravalent hydrolysates, as well as U, Cr, V, Pb, Mn, Zn, and Ba, are predominantly transported in the colloidal fraction.

Pairwise correlations further revealed two distinct geochemical associations. Nutrients and relatively labile metals (Si, P, Li, K, Rb, V, Ni, Cu) correlated strongly with DOC, suggesting common mobilization from organic-rich surface soils and plant litter followed by lateral transport along the hydrological continuum (Krickov et al., 2026). In contrast, Al correlated with refractory lithogenic elements (Ti, Y, REEs), consistent with mobilization from deeper mineral horizons or aluminosilicate weathering (Bagard et al., 2011; Vasyukova et al., 2019), and likely release from reactive suspended particulate matter (Krickov et al., 2020; Lim et al., 2024). Al showed negative correlation with labile cations and anions (DIC, Ca, Mg, P, As), possibly indicating contrasting sources and transport pathways between mineral-groundwater-derived solutes and colloid-associated lithogenic elements.

The contrasted longitudinal behavior of solutes may reflect the superposition of at least two first-order controls along the Lower Lena continuum: (*i*) progressive hydrological integration and groundwater contributions enhancing mobile, carbonate-related species (DIC, Ca, Mg, Sr, SO_4^{2-}), and (*ii*) downstream dilution and/or sedimentation of low-solubility hydrolysates and colloid-associated trivalent–tetravalent elements (Al, REEs, Ti, Th, U). In contrast, the majority of elements and DOC displayed spatial variability without a systematic northward gradient, suggesting compensation between source inputs, in-stream processing, and hydrodynamic mixing within the large-channel system.

The localized Mn anomaly in the Undyulyung River and the smaller Fe-Mn enrichments in the Bysyttakh and Molodo tributaries most likely represent distinct tributary end members rather than a basin-wide latitudinal process. Fe and Mn can be mobilized by reductive dissolution in organic-rich, poorly oxygenated floodplain, wetland, or suprapermafrost waters and then attenuated rapidly through oxidation, sorption, colloid formation, and dilution after entering the well-oxygenated Lena main stem (Loiko et al., 2017; Hirst et al., 2017; Raudina et al., 2018; Lim et al., 2024). In particular, Mn may serve as a tracer of active-layer hydrological connectivity (Ji et al., 2021), which can explain its local enrichment in some peatland-affected headwaters of the continuous permafrost zone (Krickov et al., 2026).

Colloids exert strong control on trace-element export due to their dual organic–mineral character. In Arctic and boreal rivers, DOC concentration, optical properties, molecular composition, and biodegradability may vary independently, particularly across hydrological seasons and source domains. High-molecular-weight or colloidal DOM often carries a large fraction of the terrigenous, aromatic, and chromophoric signal, whereas lower-molecular-weight fractions can be more directly linked to recent microbial processing or photochemical alteration (Guéguen et al., 2006; Fellman et al., 2010; Amon et al., 2012; Mann et al., 2012). Therefore, the 1 kDa-0.45 µm DOC fraction measured here is best viewed as an operationally defined colloidal organic-carbon pool that can stabilize trace metals and refractory elements, while not necessarily implying uniform DOC composition or reactivity along the river continuum (Novak et al., 2022). Organic ligands of humic (peat, soil) origin efficiently complex divalent transition metals, whereas associations of trivalent and tetravalent hydrolysates—including uranyl species—with Fe and Al oxyhydroxides stabilized by organic polymers represent highly effective pathways for enhancing the apparent mobility of otherwise insoluble lithogenic elements (Vasyukova et al., 2010; Krickov et al., 2019, 2025). Importantly, the colloidal organization observed in the Lower Lena—entirely located within the continuous permafrost zone—does not differ substantially from patterns reported for the Ob River (Kolesnichenko et al., 2021), western Siberian rivers spanning a permafrost gradient (Krickov et al., 2019), the permafrost-free Severnaya Dvina (Pokrovsky et al., 2010), or boreal rivers of northwestern European Russia (Ilina et al., 2016; Vasyukova et al., 2010). The proportion of colloidal forms of individual major and trace solutes within the three principal geochemical groups identified here varies by less than ±20% relative to these systems. This convergence suggests that permafrost presence alone does not fundamentally alter the colloidal pattern of large boreal and Arctic rivers during summer baseflow, despite its strong influence on hydrological routing and active-layer dynamics. A similar conclusion was reached in earlier studies of Fe-rich colloids in the Lena basin (Hirst et al., 2017).

A limitation of the present colloidal dataset is that it is based on a single operational cutoff and a limited number of samples. Although bulk dissolved concentrations remained stable during dialysis, this quality control does not prove that the original colloidal architecture was fully preserved. Ideally, dialysis bags should be deployed directly *in situ* within river or lake waters (e.g., Vasyukova et al., 2010; Pokrovsky et al., 2016a), as this minimizes potential alterations of colloidal structure during sample handling and incubation. However, such deployment was not compatible with the logistics of a continuous ship-based survey covering 1500 km of the Lena River, where prolonged equilibration times (3–5 days) at individual locations were not possible. The data therefore constrain broad partitioning between low-molecular-weight and colloidal pools, but not the internal size distribution, surface charge, aggregation state, or mineralogical/organic composition of the colloids. Furthermore, direct structural characterization of Lena River colloids was beyond the scope of the present campaign. Future work should combine dialysis or ultrafiltration with asymmetric flow field-flow fractionation, dynamic light scattering or nanoparticle tracking, zeta potential measurements, Fe redox and mineralogical speciation, and molecular-level DOM characterization by optical spectroscopy and high-resolution mass spectrometry. Such analyses would allow the Fe-Al-organic colloid model proposed here to be tested more directly.

4.2.3. Exploratory multivariate support for transport structure

PCA and pairwise correlations provided exploratory support for the dual solute-transport pattern inferred from longitudinal trends and dialysis. The first rotated component separated lithogenic, low-solubility elements (Al, Be, Ti, Ga, Y, Nb, REEs, Th) from mobile weathering-related solutes (B, SO_4, DIC, Mg, Sr), whereas the second grouped DOC with nutrients and several trace metals. Because the first two axes explained only 36% of total variance and several variables had mixed loadings, the ordination should not be interpreted as a causal classification. Its main value is that it reproduces the broad contrast between mobile, predominantly low-molecular-weight weathering products and colloid-associated lithogenic elements, consistent with pairwise correlations, dialysis results, and patterns reported from other Siberian river systems (Kolesnichenko et al., 2021; Pokrovsky et al., 2016a, 2022a, b; Krickov et al., 2019, 2025, 2026; Lim et al., 2024; Vorobyev et al., 2021b, 2024). Taken together, long-term comparisons, size fractionation, and exploratory multivariate analyses indicate that major solute export in the Lower Lena is mainly governed by dissolved weathering- and groundwater-related inputs, whereas trace-element mobility is strongly influenced by organic and organo-mineral colloids. This transport structure helps explain why bulk DOC and associated trace elements vary less along the main stem than pCO_2, although direct characterization of DOC composition and reactivity would be required to test this mechanism.

5. Conclusions

Large Arctic rivers are key regulators of lateral carbon transfer and atmospheric carbon exchange. By combining continuous in situ pCO_2 measurements, chamber-based fluxes, multivariate statistics, and size-fractionation analyses along ~1500 km of the Lower Lena main stem and its major tributaries, this study provides an integrated view of carbon dynamics and solute transport in one of the world's largest permafrost-dominated river systems.

During the post-freshet recession, pCO_2 and calculated FCO_2 decreased northward, superimposed on local variability. Fluxes were comparable to those reported for the middle Lena, the Low Ob, and other large Siberian rivers, confirming the Lena as a moderate but persistent CO_2 source during the open-water season. The highest emissions occurred in the Vilyui tributary, underlining the role of large sub-basins in regulating main stem carbon evasion. In contrast, DOC and DIC remained relatively stable along the transect, highlighting a decoupling between bulk DOC/DIC concentrations and gaseous CO_2 dynamics. The CH_4 concentration was strongly subordinate to that of CO_2 likely because of limited floodplain/anoxic connectivity during the sampled period.

Size-fractionation, correlation analysis, and PCA are consistent with dual geochemical pattern of dissolved solutes. Mobile major ions, Si, and oxyanion-forming trace elements were mainly present in truly dissolved form (< 1 kDa) and reflected groundwater connectivity and water – carbonate/silicate rock interaction. By contrast, lithogenic low-solubility elements, especially trivalent and tetravalent hydrolysates, were transported predominantly in organo-mineral colloidal form and were associated with Al, Fe, and DOC, indicating mobilization via surface and suprapermafrost flow pathways. A similar distinction between two major solute groups, based on colloidal affinity, has been reported for other Arctic and boreal rivers, suggesting that colloidal dominance of refractory elements is a generic feature of organic-rich fluvial systems. In the studied summer dataset, continuous permafrost did not appear to fundamentally alter the transport of major and trace solutes, but mainly controls hydrological pathways and exchange with deeper groundwater. Under ongoing Arctic warming, changes in discharge, vegetation, and surface-flow connectivity are therefore likely to affect Lena hydrochemistry more strongly than direct thermal effects, while winter talik development may exert stronger influence on labile solutes and inorganic carbon export.

Authors contribution: Y.Y.K., V.A.N., O.V.D., D.V.C., E.A.S., A.V.K., V.A.K carried field work ; O.S.P, Y.Y.K, S.N.V. performed the analyses; S.N.V and I.P.S. contributed to the interpretation of the results. Y.Y.K., I.P.S and O.S.P took the lead in writing the manuscript. All authors provided critical feedback and helped shape the research, analysis and manuscript.

Data availability: All primary data are presented in the Supplementary Material (Table S1).

Acknowledgements:

Partial support from Priority-2030 Programme of the TSU is acknowledged. OP was partially supported by the project PEACE of PEPR FairCarboN ANR-22-PEXF-0011. IS and DCh were partially supported by the Russian Ministry of Science and Higher Education through projects FEFF-2024-0004 and FEFF-2026-0007 to SakhGU.

Declaration of generative AI and AI-assisted technologies in the manuscript preparation process

During the preparation of the revised version of the manuscript, the authors used ChatGPT (OpenAI; GPT-5.5 Pro) to assist in reviewing and synthesizing recent research literature, organizing the manuscript into sections and subsections, improving the clarity and readability of author-prepared text, checking the manuscript for completeness and compliance with the journal's guidelines, and drafting figure captions. All AI-assisted outputs—including literature summaries, references, text, code, and visualizations—were critically reviewed, independently verified, and edited by the authors before inclusion in the manuscript. The authors take full responsibility for the accuracy, integrity, and content of the published article.

References

Ahmed, R., Prowse, T., Dibike, Y., Bonsal, B., O'Neil, H.: Recent trends in freshwater influx to the Arctic Ocean from four major Arctic-draining rivers, Water 12, 1189, https://doi.org/10.3390/w12041189, 2020.

Alin, S.R., Rasera, M.F.F.L., Salimon, C.I., Richey, J.E., Holtgrieve, G.W., Krusche, A.V., et al.: Physical controls on carbon dioxide transfer velocity and flux in low-gradient river systems and implications for regional carbon budgets, J. Geophys. Res. Biogeosci. 116, G01009, https://doi.org/10.1029/2010JG001398, 2011.

Allen, G.H., Pavelsky, T.M.: Global extent of rivers and streams, Science 361, 585–588, https://doi.org/10.1126/science.aat0636, 2018.

Amon, R. M. W., Rinehart, A. J., Duan, S., Louchouarn, P., Prokushkin, A., Guggenberger, G., Bauch, D., Stedmon, C., Raymond, P. A., Holmes, R. M., McClelland, J. W., Peterson, B. J., Walker, S. A., and Zhulidov, A. V.: Dissolved organic matter sources in large Arctic rivers, Geochim. Cosmochim. Acta, 94, 217-237, https://doi.org/10.1016/j.gca.2012.07.015, 2012.

Attermeyer, K., Catalan, N., Einarsdottir, K., Freixa, A., Groeneveld, M., Hawkes, J.A., et al.: Organic carbon processing during transport through boreal inland waters: particles as important sites, J. Geophys. Res. Biogeosci. 123, 2412–2428, https://doi.org/10.1029/2018JG004500, 2018.

Bagard, M.L., Chabaux, F., Pokrovsky, O.S., Viers, J., Prokushkin, A.S., Stille, P., Rihs, S., Schmitt, A.D., Dupré, B.: Seasonal variability of element fluxes in two Central Siberian rivers draining high latitude permafrost dominated areas, Geochim. Cosmochim. Acta 75, 3335–3357, 2011.

Bastviken, D., Tranvik, L. J., Downing, J. A., Crill, P. M., and Enrich-Prast, A.: Freshwater methane emissions offset the continental carbon sink, Science, 331, 50, https://doi.org/10.1126/science.1196808, 2011.

Beckebanze, L., Runkle, B.R.K., Walz, J., Wille, C., Holl, D., Helbig, M., Boike, J., Sachs, T., Kutzbach, L.: Lateral carbon export has low impact on the net ecosystem carbon balance of a polygonal tundra catchment, Biogeosciences 19, 3863–3876, https://doi.org/10.5194/bg-19-3863-2022, 2022.

Berezovskaya, S., Yang, D., Hinzman, L.: Long-term annual water balance analysis of the Lena River, Glob. Planet. Change 48, 84–95, https://doi.org/10.1016/j.gloplacha.2004.12.006, 2005.

Brown, J., Ferrians Jr., O.J., Heginbottom, J.A., Melnikov, E.S.: Circum-Arctic map of permafrost and ground-ice conditions, National Snow and Ice Data Center/World Data Center for Glaciology, Boulder, CO, USA, digital media, 2002.

Bussmann, I.: Distribution of methane in the Lena Delta and Buor-Khaya Bay, Russia, Biogeosciences 10, 4641–4652, https://doi.org/10.5194/bg-10-4641-2013, 2013.

Bussmann, I., Hackbusch, S., Schaal, P., and Wichels, A.: Methane distribution and oxidation around the Lena Delta in summer 2013, Biogeosciences, 14, 4985-5002, https://doi.org/10.5194/bg-14-4985-2017, 2017.

Cai, W.-J., Wang, Y.: The chemistry, fluxes, and sources of carbon dioxide in the estuarine waters of the Satilla and Altamaha Rivers, Georgia, Limnol. Oceanogr. 43, 657–668, https://doi.org/10.4319/lo.1998.43.4.0657, 1998.

Cauwet, G., Sidorov, I.: The biogeochemistry of Lena River: organic carbon and nutrients distribution, Mar. Chem. 53, 211–227, https://doi.org/10.1016/0304-4203(95)00090-9, 1996.

Chevychelov, A.P., Bosikov, N.P.: Natural conditions, In: Troeva, E.I., et al. (Eds.), The Far North. Springer, Netherlands, p. 123, https://link.springer.com/chapter/10.1007/978-90-481-3774-9_1, 2010.

Chupakov, A.V., Pokrovsky, O.S., Shirokova, L.S., Moreva, O.Y., Neverova, N.V., Chupakova, A.A., Kotova, A.I., Vorobyeva, T.Y.: High resolution multi-annual riverine fluxes of organic carbon, nutrient and trace element from the largest European Arctic river, Severnaya Dvina, Chem. Geol. 538, 119491, 2020.

Chupakov, A.V., Pokrovsky, O.S., Moreva, O.Y., Kotova, E., Vorobyeva, T.Y., Shirokova, L.S.: Export of organic carbon, nutrient and metals by the medium-size Pechora River to the Arctic Ocean, Chem. Geol. 632, 121524, https://doi.org/10.1016/j.chemgeo.2023.121524, 2023.

Cole, J.J., Prairie, Y.T., Caraco, N.F., McDowell, W.H., Tranvik, L.J., Striegl, R.G., et al.: Plumbing the global carbon cycle: integrating inland waters into the terrestrial carbon budget, Ecosystems 10, 171–184, 2007.

Cooper, L.W., McClelland, J.W., Holmes, R.M., Raymond, P.A., Gibson, J.J., Guay, C.K., Peterson, B.J.: Flow-weighted values of runoff tracers (δ18O, DOC, Ba, alkalinity) from the six largest Arctic rivers, Geophys. Res. Lett. 35, L18606, https://doi.org/10.1029/2008GL035007, 2008.

Crawford, J.T., Striegl, R.G., Wickland, K.P., Dornblaser, M.M., Stanley, E.H.: Emissions of carbon dioxide and methane from a headwater stream network of interior Alaska, J. Geophys. Res. Biogeosci. 118, 482–494, 2013.

Cuss, C.W., Grant-Weaver, I., Shotyk, W.: AF4-ICPMS with the 300 Da membrane to resolve metal-bearing ‘colloids’ <1 kDa: optimization, fractogram deconvolution, and advanced quality control, Anal. Chem. 89, 8027–8035, 2017.

Cuss, C.W., Donner, M.W., Grant-Weaver, I., Noernberg, T., Pelletier, R., Sinnatamby, R.N., Shotyk, W.: Measuring the distribution of trace elements amongst dissolved colloidal species as a fingerprint for contribution of tributaries to large boreal rivers, Sci. Total Environ. 642, 1242–1251, 2018.

Cuss, C.W., Glover, C.N., Javed, M.B., Nagel, A., Shotyk, W.: Geochemical and biological controls on the ecological relevance of total, dissolved, and colloidal forms of trace elements in large boreal rivers: review and case studies, Environ. Rev. 28, 138–163, https://doi.org/10.1139/er-2019-0014, 2020.

Dean, J.F., Meisel, O.H., Rosco, M.M., et al.: East Siberian Arctic inland waters emit mostly contemporary carbon, Nat. Commun. 11, 1627, https://doi.org/10.1038/s41467-020-15511-6, 2020.

Denfeld, B.A., Frey, K.E., Sobczak, W.V., Mann, P.J., Holmes, R.M.: Summer CO_2 evasion from streams and rivers in the Kolyma River basin, north-east Siberia, Polar Res. 32, 19704, https://doi.org/10.3402/polar.v32i0.19704, 2013.

Drake, T.W., Raymond, P.A., Spencer, R.G.M.: Terrestrial carbon inputs to inland waters: a current synthesis of estimates and uncertainty, Limnol. Oceanogr. Lett. 3, 132–142, https://doi.org/10.1002/lol2.10055, 2018.

Dudarev, O.V., Semiletov, I.P., Charkin, A.N.: Particulate material composition in the Lena River-Laptev Sea system: scales of heterogeneities, Dokl. Earth Sci. 411A, 1445–1451, 2006.

Eckhardt, T., Knoblauch, C., Kutzbach, L., Holl, D., Simpson, G., Abakumov, E., Pfeiffer, E.-M.: Partitioning net ecosystem exchange of CO_2 on the pedon scale in the Lena River Delta, Siberia, Biogeosciences 16, 1543–1562, https://doi.org/10.5194/bg-16-1543-2019, 2019.

Fellman, J. B., Hood, E., and Spencer, R. G. M.: Fluorescence spectroscopy opens new windows into dissolved organic matter dynamics in freshwater ecosystems: a review, Limnol. Oceanogr., 55, 2452-2462, https://doi.org/10.4319/lo.2010.55.6.2452, 2010.

Feng, X.J., Vonk, J.E., van Dongen, B.E., Gustafsson, Ö., Semiletov, I.P., Dudarev, O.V., Wang, Z.H., Montluçon, D.B., Wacker, L., Eglinton, T.I.: Differential mobilization of terrestrial carbon pools in Eurasian Arctic river basins, Proc. Natl. Acad. Sci. U.S.A. 110, 14168–14173, https://doi.org/10.1073/pnas.1307031110, 2013.

Franz, D., Larmanou, E., Bornemann, N., Langer, M., Boike, J., Sachs, T.: Exchange of CO_2 and CH_4 between a Siberian thaw lake and the atmosphere, In: Proceedings of the XI International Conference on Permafrost, Potsdam, 20–24 June 2016, 2016.

Frey, K.E., Smith, L.C.: Amplified carbon release from vast West Siberian peatlands by 2100, Geophys. Res. Lett. 32, L09401, https://doi.org/10.1029/2004GL022025, 2005.

Frey, K.E., Siegel, D.I., Smith, L.C.: Geochemistry of West Siberian streams and their potential response to permafrost degradation, Water Resour. Res. 43, W03406, https://doi.org/10.1029/2006WR004902, 2007.

Gautier, E., Depret, T., Costard, F., Virmoux, C., Fedorov, A., et al.: Going with the flow: hydrologic response of middle Lena River (Siberia) to climate variability and change, J. Hydrol. 557, 475–488, https://doi.org/10.1016/j.jhydrol.2017.12.034, 2018.

Gebhardt, A.C., Gaye-Haake, B., Unger, D., Lahajnar, N., Ittekkot, V.: A contemporary sediment and organic carbon budget for the Kara Sea shelf (Siberia), Mar. Geol. 220, 83–100, https://doi.org/10.1016/j.margeo.2005.06.035, 2005.

Gelfan, A., Gustafsson, D., Motovilov, Y., Arheimer, B., Kalugin, A., Krylenko, I., Lavrenov, A.: Climate change impact on the water regime of two great Arctic rivers: modelling and uncertainty issues, Clim. Change 414, 499–515, https://doi.org/10.1007/s10584-016-1710-5, 2017.

Georgiadi, A.G., Tananaev, N.I., Dukhova, L.A.: Hydrochemical conditions at the Lena River in August 2018, Oceanology 59, 797–800, https://doi.org/10.1134/S0001437019050072, 2019.

Gonçalves-Araujo, R., Stedmon, C.A., Heim, B., Dubinenkov, I., Kraberg, A., Moiseev, D., Bracher, A.: From fresh to marine waters: characterization and fate of dissolved organic matter in the Lena River delta region, Siberia, Front. Mar. Sci. 2, 108, https://doi.org/10.3389/fmars.2015.00108, 2015.

Gordeev, V.V., Sidorov, I.S.: Concentrations of major elements and their outflow into the Laptev Sea by the Lena River, Mar. Chem. 43, 33–46, 1993.

Gordeev, V.V., Martin, J.-M., Sidorov, I.S., Sidorova, M.V.: A reassessment of the Eurasian river input of water, sediment, major elements, and nutrients to the Arctic Ocean, Am. J. Sci. 296, 664–691, 1996.

Gordeev, V.V., Rachold, V., Vlasova, I.E.: Geochemical behavior of major and trace elements in suspended particulate material of the Irtysh River, the main tributary of the Ob River, Siberia, Appl. Geochem. 19, 593–610, 2004.

Gordeev, V.V., Pokrovsky, O.S., Zhulidov, A.V., Filippov, A.S., Gurtovaya, T.Y., Holmes, R.M., Kosmenko, L.S., McClelland, J.W., Peterson, B.J., Tank, S.E.: Dissolved major and trace elements in the largest Eurasian Arctic rivers: Ob, Yenisey, Lena, and Kolyma, Water 16, 316, https://doi.org/10.3390/w16020316, 2024.

Griffin, C.G., McClelland, J.W., Frey, K.E., Fiske, G., Holmes, R.M.: Quantifying CDOM and DOC in major Arctic rivers during ice-free conditions using Landsat TM and ETM+ data, Remote Sens. Environ. 209, 395–409, https://doi.org/10.1016/j.rse.2018.02.060, 2018.

Guéguen, C., Guo, L., Wang, D., Tanaka, N., and Hung, C.-C.: Chemical characteristics and origin of dissolved organic matter in the Yukon River, Biogeochemistry, 77, 139-155, https://doi.org/10.1007/s10533-005-0806-1, 2006.

Guérin, F., Abril, G., Serça, D., Delon, C., Richard, S., Delmas, R., Tremblay, A., Varfalvy, L.: Gas transfer velocities of CO2 and CH4 in a tropical reservoir and its river downstream, J. Mar. Syst. 66, 161–172, https://doi.org/10.1016/j.jmarsys.2006.03.019, 2007.

Hirst, C., Andersson, P.S., Shaw, S., Burke, I.T., Kutscher, L., Murphy, M.J., Maximov, T., Pokrovsky, O.S., Mörth, C.-M., Porcelli, D.: Characterisation of Fe-bearing particles and colloids in the Lena River basin, NE Russia, Geochim. Cosmochim. Acta 213, 553–573, https://doi.org/10.1016/j.gca.2017.07.012, 2017.

Hirst, K., Andersson, P., Kooijman, E., Kutscher, L., Maximov, T., Mörth, C.-M., Porcelli, D.: Iron isotopes reveal the sources of Fe-bearing particles and colloids in the Lena River basin, Geochim. Cosmochim. Acta 269, 678–692, https://doi.org/10.1016/j.gca.2019.11.004, 2020.

Holmes, R.M., Peterson, B.J., Gordeev, V.V., Zhulidov, A.V., Meybeck, M., Lammers, R.B., Vörösmarty, C.J.: Flux of nutrients from Russian rivers to the Arctic Ocean: can we establish a baseline against which to judge future changes? Water Resour, Res. 36, 2309–2320, 2000.

Holmes, R.M., Peterson, B.J., Zhulidov, A.V., Gordeev, V.V., Makkaveev, P.N., Stunzhas, P.A., Kosmenko, L.S., Köhler, G.H., Shiklomanov, A.I.: Nutrient chemistry of the Ob' and Yenisey Rivers, Siberia: results from June 2000 expedition and evaluation of long-term data sets, Mar. Chem. 75, 219–227, 2001.

Holmes, R.M., Coe, M.T., Fiske, G.J., Gurtovaya, T., McClelland, J.W., Shiklomanov, A.I., Spencer, R.G.M., Tank, S.E., Zhulidov, A.V.: Climate change impacts on the hydrology and biogeochemistry of Arctic rivers, In: Goldman, C.R., Kumagai, M., Robarts, R.D. (Eds.), Climatic Changes and Global Warming of Inland Waters: Impacts and Mitigation for Ecosystems and Societies. John Wiley & Sons, pp. 1–26, 2013.

Hopkinson, C.S.: Shallow-water benthic and pelagic metabolism, Mar. Biol. 87, 19–32, https://doi.org/10.1007/BF00397002, 1985.

Horan, K., Hilton, R.G., Dellinger, M., Tipper, E., Galy, V., Calmels, D., Selby, D., Gaillardet, J., Ottley, C.J., Parsons, D.R., Burton, K.W.: Carbon dioxide emissions by rock organic carbon oxidation and the net geochemical carbon budget of the Mackenzie River Basin, Am. J. Sci. 319, 473–499, https://doi.org/10.2475/06.2019.02, 2019.

Hotchkiss, E., Hall Jr., R., Sponseller, R., et al.: Sources of and processes controlling CO2 emissions change with the size of streams and rivers, Nat. Geosci. 8, 696–699, https://doi.org/10.1038/ngeo2507, 2015.

Huh, Y., Tsoi, M.Y., Zaitsev, A., Edmond, J.M.: The fluvial geochemistry of the rivers of eastern Siberia: I, Tributaries of the Lena River draining the sedimentary platform of the Siberian Craton. Geochim. Cosmochim. Acta 62, 1657–1676, https://doi.org/10.1016/S0016-7037(98)00107-0, 1998a.

Huh, Y., Panteleyev, G., Babich, O., Zaitsev, A., Edmond, J.M.: The fluvial geochemistry of the rivers of Eastern Siberia: II, Tributaries of the Lena, Omoloy, Yana, Indigirka, Kolyma, and Anadyr draining the collisional/accretionary zone of the Verkhoyansk and Cherskiy ranges. Geochim. Cosmochim. Acta 62, 5063–5075, 1998b.

Huh, Y., Edmond, J.M.: The fluvial geochemistry of the rivers of Eastern Siberia: III, Tributaries of the Lena and Anabar draining the basement terrain of the Siberian Craton and the Trans-Baikal Highlands. Geochim. Cosmochim. Acta 63, 967–987, https://doi.org/10.1016/S0016-7037(99)00045-9, 1999.

Humborg, C., Mörth, C.-M., Sundbom, M., Borg, H., Blenckner, T., Giesler, R., Ittekkot, V.: CO2 supersaturation along the aquatic conduit in Swedish watersheds as constrained by terrestrial respiration, aquatic respiration and weathering, Glob. Change Biol. 16, 1966–1978, https://doi.org/10.1111/j.1365-2486.2009.02092.x, 2010.

Ilina, S. M., Drozdova, O. Y., Lapitsky, S. A., Alekhin, Yu. V., Demin, V. V., Zavgorodnaya, Yu. A., Shirokova, L. S., Viers, J., Pokrovsky, O. S. Size fractionation and optical properties of dissolved organic matter in the continuum soil solution-bog-river and terminal lake of a boreal watershed. Organic Geochemistry, 66, 14–24, 2014.

Ilina, S.M., Lapitsky, S.A., Alekhin, Y.V., Viers, J., Benedetti, M., Pokrovsky, O.S.: Speciation, size fractionation and transport of trace element in the continuum soil water–mire–lake–river–large oligotrophic lake of a subarctic watershed, Aquat. Geochem. 22, 65–95, 2016.

Jähne, B., Heinz, G., Dietrich, W.: Measurement of the diffusion coefficients of sparingly soluble gases in water, J. Geophys. Res. Oceans 92, 10767–10776, https://doi.org/10.1029/JC092iC10p10767, 1987.

Ji, X., Abakumov, E., Polyakov, V., Xie, X.: Mobilization of geochemical elements to surface water in the active layer of permafrost in the Russian Arctic, Water Resources Research 57, e2020WR028269. https://doi.org/10.1029/2020WR028269, 2021.

Johnson, M.S., Billett, M.F., Dinsmore, K.J., Wallin, M., Dyson, K.E., Jassal, R.S.: Direct and continuous measurement of dissolved carbon dioxide in freshwater aquatic systems: method and applications, Ecohydrology 3, 68–78, https://doi.org/10.1002/eco, 2009.

Juhls, B., Stedmon, C.A., Morgenstern, A., Meyer, H., Hölemann, J., Heim, B., Povazhnyi, V., Overduin, P.P.: Identifying drivers of seasonality in Lena River biogeochemistry and dissolved organic matter fluxes, Front. Environ. Sci. 8, 53, https://doi.org/10.3389/fenvs.2020.00053, 2020.

Juhls, B., Morgenstern, A., Hölemann, J., Eulenburg, A., Heim, B., Miesner, F., Grotheer, H., Mollenhauer, G., Meyer, H., Erkens, E., Gehde, F.Y., Antonova, S., Chalov, S., Tereshina, M., Erina, O., Fingert, E., Abramova, E., Sanders, T., Lebedeva, L., Torgovkin, N., Maksimov, G., Povazhnyi, V., Gonçalves-Araujo, R., Wünsch, U., Chetverova, A., Opfergelt, S., Overduin, P.P.: Lena River biogeochemistry captured by a 4.5-year high-frequency sampling program, Earth Syst. Sci. Data 17, 1–28, https://doi.org/10.5194/essd-17-1-2025, 2025.

Karlsson, J., Serikova, S., Rocher-Ros, G., Denfeld, B., Vorobyev, S.N., Pokrovsky, O.S.: Carbon emission from Western Siberian inland waters, Nat. Commun. 12, 825, https://doi.org/10.1038/s41467-021-21054-1, 2021.

Kipp, L.E., Henderson, P.B., Wang, Z.A., Charrette, M.A.: Deltaic and estuarine controls on Mackenzie River solute fluxes to the Arctic Ocean, Estuar. Coasts 43, 1992–2014, https://doi.org/10.1007/s12237-020-00739-8, 2020.

Kolesnichenko, I., Kolesnichenko, L.G., Vorobyev, S.N., Shirokova, L.S., Semiletov, I.P., Dudarev, O.V., Vorobev, R.S., Shavrina, U., Kirpotin, S.N., Pokrovsky, O.S.: Landscape, soil, lithology, climate and permafrost control on dissolved carbon, major and trace elements in the Ob River, Western Siberia, Water 13, 3189, https://doi.org/10.3390/w13223189, 2021.

Krickov, I.V., Pokrovsky, O.S., Manasypov, R.M., Lim, A.G., Shirokova, L.S., Viers, J.: Colloidal transport of carbon and metals by western Siberian rivers during different seasons across a permafrost gradient, Geochim. Cosmochim. Acta 265, 221–241, https://doi.org/10.1016/j.gca.2019.08.041, 2019.

Krickov, I.V., Lim, A.G., Manasypov, R.M., Loiko, S.V., Vorobyev, S.N., Shevchenko, V.P., Dara, O.M., Gordeev, V.V., Pokrovsky, O.S.: Major and trace elements in suspended matter of western Siberian rivers: first assessment across permafrost zones and landscape parameters of watersheds, Geochim. Cosmochim. Acta 269, 429–450, https://doi.org/10.1016/j.gca.2019.11.005, 2020.

Krickov, I.V., Lim, A.G., Korets, M., Shirokova, L.S., Karlsson, J., Pokrovsky, O.S.: Environmental controllers for carbon emission and concentration patterns in Siberian rivers during different seasons, Sci. Total Environ. 859, 160202, https://doi.org/10.1016/j.scitotenv.2022.160202, 2023.

Krickov, I.V., Vorobyev, S.N., Kolesnichenko, L.G., Kolesnichenko, Y., Zinchenko, D., Shirokova, L.S., Pokrovsky, O.S.: Export fluxes of dissolved, colloidal and particulate organic carbon, major and trace elements from the Ob River and its tributaries across seasons, Water Res. 275, 123221, https://doi.org/10.1016/j.watres.2025.123221, 2025.

Krickov, I.V., Loiko, S.V., Lim, A., Kuzmina, D.M., Istigechev, G.I., Shirokova, L.S., Pupyshev, Y.S., Pokrovsky, O.S.: Hydrological continuums across climate and permafrost gradients: spatial patterns of organic carbon, greenhouse gases, and major and trace elements, Water Res. 294, 125507, https://doi.org/10.1016/j.watres.2026.125507, 2026.

Kruse, S., Gerdes, A., Kath, N.J., Epp, L.S., Stoof-Leichsenring, K.R., Pestryakova, L.A., Herzschuh, U.: Dispersal distances and migration rates at the arctic treeline in Siberia – a genetic and simulation-based study, Biogeosciences 16, 1211–1224, https://doi.org/10.5194/bg-16-1211-2019, 2019.

Kutscher, L., Mörth, C.-M., Porcelli, D., Hirst, C., Maximov, T.C., Petrov, R.E., Andersson, P.S.: Spatial variation in concentration and sources of organic carbon in the Lena River, Siberia, J. Geophys. Res. Biogeosci. 122, 1999–2014, https://doi.org/10.1002/2017JG003858, 2017.

Kutzbach, L., Wille, C., Pfeiffer, E.-M.: The exchange of carbon dioxide between wet arctic tundra and the atmosphere at the Lena River Delta, Northern Siberia, Biogeosciences 4, 869–890, https://doi.org/10.5194/bg-4-869-2007, 2007.

Kuzmin, M.I., Tarasova, E.N., Bychinskii, V.A., Karabanov, E.B., Mamontov, A.A., Mamontova, E.A.: Hydrochemical regime components of Lena water, Water Resour. 36, 418–430, https://doi.org/10.1134/S0097807809040058, 2009.

Lara, R.J., Rachold, V., Kattner, G., Hubberten, H.-W., Guggenberger, G., Annelie, S., Thomas, D.N.: Dissolved organic matter and nutrients in the Lena River, Siberian Arctic: characteristics and distribution, Mar. Chem. 59, 301–309, https://doi.org/10.1016/S0304-4203(97)00076-5, 1998.

Lauerwald, R., Laruelle, G.G., Hartmann, J., Ciais, P., Regnier, P.A.G.: Spatial patterns in CO2 evasion from the global river network, Global Biogeochem. Cycles 29, 534–554, https://doi.org/10.1002/2014GB004941, 2015.

Leith, F.I., Garnett, M.H., Dinsmore, K.J., Billett, M.F., Heal, K.V.: Source and age of dissolved and gaseous carbon in a peatland-riparian-stream continuum: a dual isotope (14C and δ13C) analysis, Biogeochemistry 119, 415–433, https://doi.org/10.1007/s10533-014-9977-y, 2014.

Leith, F.I., Dinsmore, K.J., Wallin, M.B., Billett, M.F., Heal, K.V., Laudon, H., Öquist, M.G., Bishop, K.: Carbon dioxide transport across the hillslope–riparian–stream continuum in a boreal headwater catchment, Biogeosciences 12, 1–12, https://doi.org/10.5194/bg-12-1-2015, 2015.

Lim, A. G., Krickov, I. V., Vorobyev, S. N., Korets, M. A., Kopysov, S., Shirokova, L. S., Karlsson, J., and Pokrovsky, O. S.: Carbon emission and export from the Ket River, western Siberia, Biogeosciences, 19, 5859-5877, https://doi.org/10.5194/bg-19-5859-2022, 2022.

Lim, A.G., Krickov, I.V., Pokrovsky, O.S.: Organic carbon, major and trace element release from and adsorption onto riverine particulate suspended matter: experimental approach, Sci. Total Environ. 948, 174735, https://doi.org/10.1016/j.scitotenv.2024.174735, 2024.

Lobbes, J.M., Fitznar, H.P., Kattner, G.: Biogeochemical characteristics of the dissolved and particulate organic matter in Russian rivers entering the Arctic Ocean, Geochim. Cosmochim. Acta 64, 2973–2983, 2000.

Loiko, S.V., Pokrovsky, O.S., Raudina, T.V., Lim, A., Kolesnichenko, L.G., Shirokova, L.S., Vorobyev, S.N., Kirpotin, S.N.: Abrupt permafrost collapse enhances organic carbon, CO2, nutrient and metal release into surface waters, Chem. Geol. 471, 153–165, 2017.

Mann, P. J., Davydova, A., Zimov, N., Spencer, R. G. M., Davydov, S., Bulygina, E., Zimov, S., and Holmes, R. M.: Controls on the composition and lability of dissolved organic matter in Siberia's Kolyma River basin, J. Geophys. Res. Biogeosci., 117, G01028, https://doi.org/10.1029/2011JG001798, 2012.

Marie, D., Partensky, F., Vaulot, D., Brussaard, C.: Enumeration of phytoplankton, bacteria, and viruses in marine samples, Curr. Protoc. Cytom. 10, 11111–111115, https://doi.org/10.1002/0471142956.cy1111s10, 1999.

Mavromatis, V.M., Porcelli, D., Andersson, P., Korets, M., Pokrovsky, O.S.: Lithological controls of the Mg isotope composition of the Lena River and its tributaries across seasons, Chem. Geol. 648, 121957, https://doi.org/10.1016/j.chemgeo.2024.121957, 2024.

McClelland, J.W., Holmes, R.M., Peterson, B.J., Strieglitz, M.: Increasing river discharge in the Eurasian Arctic: consideration of dams, permafrost thaw, and fires as potential agents of change, J. Geophys. Res. Atmos. 109, D18102, https://doi.org/10.1029/2004JD004583, 2004.

McClelland, J.W., Déry, S.J., Peterson, B.J., Holmes, R.M., Wood, E.F.: A pan-Arctic evaluation of changes in river discharge during the latter half of the 20th century, Geophys. Res. Lett. 33, L06715, https://doi.org/10.1029/2006GL025753, 2006.

Mu, C., Li, K., Liu, S., et al.: Recent intensified riverine CO_2 emission across the Northern Hemisphere permafrost region, Nat. Commun. 16, 3616, https://doi.org/10.1038/s41467-025-58716-3, 2025.

Murphy, M., Porcelli, D., Pogge von Strandmann, P., Hirst, K., Kutscher, L., Katchinoff, J., Mörth, C.-M., Maximov, T., Andersson, P.: Tracing silicate weathering processes in the permafrost-dominated Lena River watershed using lithium isotopes, Geochim. Cosmochim. Acta 245, 154–171, https://doi.org/10.1016/j.gca.2018.10.024, 2018.

Novak, M. G., Mannino, A., Clark, J. B., Hernes, P., Tzortziou, M., Spencer, R. G. M., Kellerman, A. M., and Grunert, B.: Arctic biogeochemical and optical properties of dissolved organic matter across river to sea gradients, Front. Mar. Sci., 9, 949034, https://doi.org/10.3389/fmars.2022.949034, 2022.

Ogneva, O., Mollenhauer, G., Juhls, B., Sanders, T., Palmtag, J., Fuchs, M., Grotheer, H., Mann, P.J., Strauss, J.: Particulate organic matter in the Lena River and its delta: from the permafrost catchment to the Arctic Ocean, Biogeosciences 20, 1423–1441, https://doi.org/10.5194/bg-20-1423-2023, 2023.

Opfergelt, S., Gaspard, F., Hirst, C., Monin, L., Juhls, B., Morgenstern, A., Angelopoulos, M., and Overduin, P. P.: Frazil ice changes winter biogeochemical processes in the Lena River, Commun. Earth Environ., 5, 738, https://doi.org/10.1038/s43247-024-01884-9, 2024.

Pipko, I.I., Pugach, S.P., Savichev, O.G., Repina, I.A., Shakhova, N.E., Moiseeva, Yu.A., Barskov, K.V., Sergienko, V.I., Semiletov, I.P.: Dynamics of dissolved inorganic carbon and CO2 fluxes between the water and the atmosphere in the main channel of the Ob River, Dokl. Chem. 484, 52–57, https://doi.org/10.1134/S0012500819020101, 2019.

Pipko, I.I., Pugach, S.P., Dudarev, O.V., Charkin, A.N., Semiletov, I.P.: Carbonate parameters of the Lena River: characteristics and distribution, Geochem. Int. 48, 1131–1137, https://doi.org/10.1134/S0016702910110078, 2010.

Pipko, I. I., Pugach, S. P., Shcherbakova, K. P., and Semiletov, I. P.: Optical signatures of dissolved organic matter in the Siberian Rivers during summer season, J. Hydrol., 620, 129468, https://doi.org/10.1016/j.jhydrol.2023.129468, 2023.

Pokrovsky, O.S., Viers, J., Shirokova, L.S., Shevchenko, V.P., Filippov, A.S., Dupré, B.: Dissolved, suspended, and colloidal fluxes of organic carbon, major and trace elements in Severnaya Dvina River and its tributary, Chem. Geol. 273, 136–149, 2010.

Pokrovsky, O.S., Manasypov, R.M., Loiko, S.V., Shirokova, L.S.: Organic and organo-mineral colloids in discontinuous permafrost zone, Geochim. Cosmochim. Acta 188, 1–20, 2016a.

Pokrovsky, O.S., Manasypov, R.M., Loiko, S., Krickov, I.A., Kopysov, S.G., Kolesnichenko, L.G., Vorobyev, S.N., Kirpotin, S.N.: Trace element transport in western Siberia rivers across a permafrost gradient, Biogeosciences 13, 1877–1900, 2016b.

Pokrovsky, O.S., Lim, A.G., Krickov, I.V., Korets, M.A., Shirokova, L.S., Vorobyev, S.N.: Hydrochemistry of medium-size pristine rivers in boreal and subarctic zone: disentangling effect of landscape parameters across a permafrost, climate, and vegetation gradient, Water 14, 2250, https://doi.org/10.3390/w14142250, 2022a.

Pokrovsky, O.S., Manasypov, R.M., Chupakov, A.V., Kopysov, S.: Element transport in the Taz River, western Siberia, Chem. Geol. 614, 121180, https://doi.org/10.1016/j.chemgeo.2022.121180, 2022b.

Qin, J., Huh, Y., Edmond, J.M., Du, G., Ran, J.: Chemical and physical weathering in the Min Jiang, a headwater tributary of the Yangtze River, Chem. Geol. 227, 53–69, https://doi.org/10.1016/j.chemgeo.2005.09.011, 2006.

Rachold, V., Alabyan, A., Hubberten, H.-W., Korotaev, V.N., Zaitsev, A.A.: Sediment transport to the Laptev Sea: hydrology and geochemistry of the Lena River, Polar Res. 15, 183–196, https://doi.org/10.3402/polar.v15i2.6646, 1996.

Raudina, T.V., Loiko, S.V., Lim, A., Manasypov, R.M., Shirokova, L.S., Istigechev, G.I., Kuzmina, D.M., Kulizhsky, S.P., Vorobyev, S.N., Pokrovsky, O.S.: Permafrost thaw and climate warming may decrease the CO_2, carbon, and metal concentration in peat soil waters of the Western Siberia Lowland, Sci. Total Environ. 634, 1004–1023, 2018.

Raudina, T.V., Loiko, S., Kuzmina, D.M., Shirokova, L.S., Kulizhsky, S.P., Golovatskaya, E.A., Pokrovsky, O.S.: Colloidal organic carbon and trace elements in peat porewaters across a permafrost gradient in Western Siberia, Geoderma 390, 114971, https://doi.org/10.1016/j.geoderma.2021.114971, 2021.

Raymond, P.A., Hartmann, J., Lauerwald, R., Sobek, S., McDonald, C., Hoover, M., Butman, D., Striegl, R., Mayorga, E., Humborg, C., Kortelainen, P., Dürr, H., Meybeck, M., Ciais, P., Guth, P.: Global carbon dioxide emissions from inland waters, Nature 503, 355–359, https://doi.org/10.1038/nature12760, 2013.

Rocher-Ros, G., Sponseller, R.A., Lidberg, W., Mörth, C.-M., Giesler, R.: Landscape process domains drive patterns of CO_2 evasion from river networks, Limnol. Oceanogr. Lett. 4, 87–95, https://doi.org/10.1002/lol2.10108, 2019.

Rocher-Ros, G., Stanley, E.H., Loken, L.C., et al.: Global methane emissions from rivers and streams, Nature 621, 530–535, https://doi.org/10.1038/s41586-023-06344-6, 2023.

Sachs, T., Wille, C., Boike, J., Kutzbach, L.: Environmental controls on ecosystem-scale CH_4 emission from polygonal tundra in the Lena River Delta, Siberia, J. Geophys. Res. Biogeosci. 113, G00A03, https://doi.org/10.1029/2007JG000505, 2008.

Savenko, A.V., Savenko, V.S.: Trace element composition of the dissolved matter runoff of the Russian Arctic rivers, Water 16, 565, https://doi.org/10.3390/w16040565, 2024.

Schuur, E.A.G., McGuire, A.D., Schädel, C., Grosse, G., Harden, J.W., Hayes, D.J., Hugelius, G., Koven, C.D., Kuhry, P., Lawrence, D.M., Natali, S.M., Olefeldt, C., Romanovsky, V.E., Schaefer, K., Turetsky, M.R., Treat, C.C., Vonk, J.E.: Climate change and the permafrost carbon feedback, Nature 520, 171–179, https://doi.org/10.1038/nature14338, 2015.

Semiletov, I.P.: Aquatic sources and sinks of CO_2 and CH_4 in the polar regions, J. Atmos. Sci. 56, 286–306, https://doi.org/10.1175/1520-0469(1999)056<0286:ASASOC>2.0.CO;2, 1999.

Semiletov, I.P., Pipko, I.I., Shakhova, N.E., Dudarev, O.V., Pugach, S.P., Charkin, A.N., McRoy, C.P., Kosmach, D., Gustafsson, Ö.: Carbon transport by the Lena River from its headwaters to the Arctic Ocean, with emphasis on fluvial input of terrestrial particulate organic carbon vs, carbon transport by coastal erosion. Biogeosciences 8, 2407–2426, https://doi.org/10.5194/bg-8-2407-2011, 2011.

Serikova, S., Pokrovsky, O.S., Ala-aho, P., Kazantsev, V., Kirpotin, S.N., Kopysov, S.G., Krickov, I.V., Laudon, H., Manasypov, R.M., Shirokova, L.S., Soulsby, C., Tetzlaff, D., Karlsson, J.: High riverine CO_2 emissions at the permafrost boundary of Western Siberia, Nat. Geosci. 11, 825–829, https://doi.org/10.1038/s41561-018-0218-1, 2018.

Serikova, S., Pokrovsky, O.S., Laudon, H., Krickov, I.V., Lim, A.G., Manasypov, R.M., Karlsson, J.: C emissions from lakes across permafrost gradient of Western Siberia, Nat. Commun. 10, 1552, https://doi.org/10.1038/s41467-019-09592-1, 2019.

Siewert, M.B., Hugelius, G., Heim, B., Faucherre, S.: Landscape controls and vertical variability of soil organic carbon storage in permafrost-affected soils of the Lena River Delta, Catena 147, 725–741, https://doi.org/10.1016/j.catena.2016.07.048, 2016.

Smith, L.C., Pavelsky, T.M.: Estimation of river discharge, propagation speed, and hydraulic geometry from space: Lena River, Siberia, Water Resour. Res. 44, W03427, https://doi.org/10.1029/2007WR006133, 2008.

Spence, J., Telmer, K.: The role of sulfur in chemical weathering and atmospheric CO2 fluxes: evidence from major ions, δ13CDIC, and δ34SSO4 in rivers of the Canadian Cordillera, Geochim. Cosmochim. Acta 69, 5441–5458, https://doi.org/10.1016/j.gca.2005.07.011, 2005.

Stanley, E. H., Casson, N. J., Christel, S. T., Crawford, J. T., Loken, L. C., and Oliver, S. K.: The ecology of methane in streams and rivers: patterns, controls, and global significance, Ecol. Monogr., 86, 146–171, https://doi.org/10.1890/15-1027.1, 2016.

Stolpe, B., Guo, L., Shiller, A.: Binding and transport of rare earth elements by organic and iron-rich nanocolloids in Alaskan rivers, as revealed by field-flow fractionation and ICP-MS, Geochim. Cosmochim. Acta 106, 446–462, 2013a.

Stolpe, B., Guo, L., Shiller, A.M., Aiken, G.R.: Abundance, size distributions and trace-element binding of organic and iron-rich nanocolloids in Alaskan rivers, as revealed by field-flow fractionation and ICP-MS, Geochim. Cosmochim. Acta 105, 221–239, 2013b.

Striegl, R.G., Dornblaser, M.M., McDonald, C.P., Rover, J.R., Stets, E.G.: Carbon dioxide and methane emissions from the Yukon River system, Global Biogeochem. Cycles 26, GB0E05, https://doi.org/10.1029/2012GB004306, 2012.

Sun, X., Mörth, C.-M., Porcelli, D., Kutscher, L., Hirst, C., Murphy, M.J., Maximov, T., Petrov, R.E., Humborg, C., Schmitt, M., Andersson, P.S.: Stable silicon isotopic compositions of the Lena River and its tributaries: implications for silicon delivery to the Arctic Ocean, Geochim. Cosmochim. Acta 241, 120–133, https://doi.org/10.1016/j.gca.2018.08.044, 2018.

Suzuki, K., Matsuo, K., Yamazaki, D., Ichii, K., Iijima, Y., Papa, F., Yanagi, Y., Hiyama, T.: Hydrological variability and changes in the Arctic circumpolar tundra and the three largest Pan-Arctic river basins from 2002 to 2016, Remote Sens. 10, 402, https://doi.org/10.3390/rs10030402, 2018.

Tananaev, N., Lotsari, E.: Defrosting northern catchments: fluvial effects of permafrost degradation, Earth-Sci. Rev. 228, 103996, https://doi.org/10.1016/j.earscirev.2022.103996, 2022.

Tananaev, N.I., Makarieva, O.M., Lebedeva, L.S.: Trends in annual and extreme flows in the Lena River basin, Northern Eurasia, Geophys. Res. Lett. 43, 10764–10772, https://doi.org/10.1002/2016GL070796, 2016.

Tank, S.E., Raymond, P.A., Striegl, R.G., McClelland, J.W., Holmes, R.M., Fiske, G.J., Peterson, B.J.: A land-to-ocean perspective on the magnitude, source and implication of DIC flux from major Arctic rivers to the Arctic Ocean, Global Biogeochem. Cycles 26, GB4018, 2012.

Tank, S.E., McClelland, J.W., Spencer, R.G.M., Shiklomanov, A.I., Suslova, A., Moatar, F., Amon, R.M.W., Cooper, L.W., Elias, G., Gordeev, V.V., Guay, C., Gurtovaya, T.Y., Kosmenko, L.S., Mutter, E.A., Peterson, B.J., Peucker-Ehrenbrink, B., Raymond, P.A., Schuster, P.F., Scott, L., Staples, R., Striegl, R.G., Tretiakov, M., Zhulidov, A.V., Zimov, N., Zimov, S., Holmes, R.M.:

Recent trends in the chemistry of major northern rivers signal widespread Arctic change, Nat. Geosci. 16, 789–796, https://doi.org/10.1038/s41561-023-01247-7, 2023.

Vachon, D., Prairie, Y.T., Cole, J.J.: The relationship between near-surface turbulence and gas transfer velocity in freshwater systems and its implications for floating chamber measurements of gas exchange, Limnol. Oceanogr. 55, 1723–1732, https://doi.org/10.4319/lo.2010.55.4.1723, 2010.

Vasyukova, E.V., Pokrovsky, O.S., Viers, J., Oliva, P., Dupré, B., Martin, F., Candaudap, F.: Trace elements in organic- and iron-rich surficial fluids of the boreal zone: assessing colloidal forms via dialysis and ultrafiltration, Geochim. Cosmochim. Acta 74, 449–468, 2010.

Vasyukova, E.V., Oliva, P., Viers, J., Martin, F., Dupré, B., Pokrovsky, O.S.: Chemical weathering of mafic rocks in boreal subarctic environment (North-West Russia) under influence of glacial moraine deposits, Chem. Geol. 509, 115–133, 2019.

Vonk, J.E., Tank, S.E., Mann, P.J., Spencer, R.G.M., Treat, C.C., Striegl, R.G., Abbott, B.W., Wickland, K.P.: Biodegradability of dissolved organic carbon in permafrost soils and aquatic systems: a meta-analysis, Biogeosciences 12, 6915–6930, https://doi.org/10.5194/bg-12-6915-2015, 2015.

Vonk, J.E., Tank, S.E., Walvoord, M.A.: Integrating hydrology and biogeochemistry across frozen landscapes, Nat. Commun. 10, 1–4, https://doi.org/10.1038/s41467-019-13361-5, 2019.

Vonk, J., Speetjens, N.J., Poste, A.: Small watersheds may play a disproportionate role in Arctic land-ocean fluxes, Nat. Commun. 14, https://doi.org/10.1038/s41467-023-39209-7, 2023.

Vorobyev, S.N., Pokrovsky, O.S., Kolesnichenko, L.G., Manasypov, R.M., Shirokova, L.S., Karlsson, J., Kirpotin, S.N.: Biogeochemistry of dissolved carbon, major, and trace elements during spring flood periods on the Ob River, Hydrol. Process. 33, 1579–1594, https://doi.org/10.1002/hyp.13424, 2019.

Vorobyev, S.N., Karlsson, J., Kolesnichenko, Y.Y., Korets, M., Pokrovsky, O.S.: Fluvial carbon dioxide emission from the Lena River basin during the spring flood, Biogeosciences 18, 4919–4936, https://doi.org/10.5194/bg-18-4919-2021, 2021a.

Vorobyev, S.N., Kolesnichenko, Y., Korets, M., Pokrovsky, O.S.: Testing landscape, climate and lithology impact on hydrochemical features of the Lena River and its tributaries, Water (MDPI) 13, Art No 2093, https://doi.org/10.3390/w13152093, 2021b.

Vorobyev, S.N., Kolesnichenko, Y., Karlsson, J., Pokrovsky, O.S.: Carbon emission from the Lower Ob River floodplain during spring flood, Sci. Total Environ. 954, 176294, https://doi.org/10.1016/j.scitotenv.2024.176294, 2024.

Wanninkhof, R.: Relationship between wind speed and gas exchange over the ocean, J. Geophys. Res. 97, 7373–7382, 1992.

Ward, C.P., Nalven, S.G., Crump, B.C., Kling, G.W., Cory, R.M.: Photochemical alteration of organic carbon draining permafrost soils shifts microbial metabolic pathways and stimulates respiration, Nat. Commun. 8, 772, https://doi.org/10.1038/s41467-017-00759-2, 2017.

Wegner, R., Fiencke, C., Knoblauch, C., Sauerland, L., Beer, C.: Rapid permafrost thaw removes nitrogen limitation rising the potential of N2O emissions, EGU General Assembly 2022, Vienna, Austria, 23–27 May 2022, EGU22-11181, https://doi.org/10.5194/egusphere-egu22-11181, 2022.

Wild, B., Andersson, A., Bröder, L., Vonk, J., Hugelius, G., McClelland, J.W., Song, W., Raymond, P.A., Gustafsson, Ö.: Rivers across the Siberian Arctic unearth the patterns of carbon release from the thawing permafrost, Proc. Natl. Acad. Sci. U.S.A. 116, 10280–10285, https://doi.org/10.1073/pnas.1811797116, 2019.

Wu, L., Huh, Y.: Dissolved reactive phosphorus in large rivers of East Asia, Biogeochemistry 85, 263–288, https://doi.org/10.1007/s10533-007-9133-z, 2007.

Yang, D.Q., Kane, D.L., Hinzman, L.D., Zhang, X.B., Zhang, T.J., Ye, H.C.: Siberian Lena River hydrological regime and recent change, J. Geophys. Res. Atmos. 107, 4694, https://doi.org/10.1029/2002JD002542, 2002.

Yamamoto, S., Alcauskas, J.B., Crozier, T.E.: Solubility of methane in distilled water and seawater, J. Chem. Eng. Data 21, 78–80, https://doi.org/10.1021/je60068a029, 1976.

Ye, B., Yang, D., Zhang, Z., Kane, D.L.: Variation of hydrological regime with permafrost coverage over Lena basin in Siberia, J. Geophys. Res. 114, D07102, https://doi.org/10.1029/2008JD010537, 2009.

Yeghicheyan, D., Aubert, D., Bouhnik-Le Coz, M., Chmeleff, J., Delpoux, S., Djouraev, I., Granier, G., Lacan, F., Piro, J.-L., Rousseau, T., Cloquet, C., Marquet, A., Menniti, C., Pradoux, C., Freydier, R., Vieira da Silva-Filho, E., Suchorski, K.: A new interlaboratory characterisation of silicon, rare earth elements and twenty-two other trace element concentrations in the natural river water certified reference material SLRS-6 (NRC-CNRC), Geostand. Geoanal. Res. 43, 475–496, https://doi.org/10.1111/ggr.12268, 2019.

Yoon, T.K., Jin, H., Oh, N.-H., Park, J.-H.: Technical note: assessing gas equilibration systems for continuous pCO_2 measurements in inland waters, Biogeosciences 13, 3915–3930, https://doi.org/10.5194/bg-13-3915-2016, 2016.

Zhang, T., Frauenfeld, O.W., Serreze, M.C., Etringer, A., Oelke, C., et al.: Spatial and temporal variability in active layer thickness over the Russian Arctic drainage basin, J. Geophys. Res. 110, D16101, https://doi.org/10.1029/2004JD005642, 2005.

Zhang, L., Bufe, A., Dean, J. F., Rocher-Ros, G., Sponseller, R. A., Stanley, E. H., Karlsson, J., Butman, D. E., Liu, R., Hou, L., Ding, J., Piao, S., Xia, X., and Battin, T. J.: Rock weathering can counteract river CO_2 emissions induced by permafrost thaw, Nature, 655, 125-132, https://doi.org/10.1038/s41586-026-10664-8, 2026.

Table 1. Hydrochemical parameters of the Lena River main stem averaged across the entire transect from Yakutsk to Kyusyur. Elemental concentrations (Li to U) are in µg/L.

Parameter	N	Mean	Std.Dev.	Median	Minimum	Maximum
pH	19	7.19	0.19	7.18	6.78	7.70
T_{water}, °C	26	17.56	1.32	17.60	15.30	20.20
O_2, mg/L	26	9.25	0.35	9.19	8.61	9.92
pCO_2, µatm	26	1019	419	892	609	2646
FCO_2, g C m^{-2} d^{-1}	12	0.33	0.20	0.25	0.11	0.68
CH_4, µmol/L	26	0.22	0.44	0.08	0.02	2.20
E.C., µS/cm	26	114	13	115	82	145
DIC, mg/L	26	8.42	2.66	8.47	4.07	18.45
DOC, mg/L	26	7.54	2.74	7.19	5.47	20.30
F-, mg/L	26	0.0665	0.02	0.07	0.03	0.12
Cl-, mg/L	26	3.52	2.13	3.41	0.60	9.71
Br-, mg/L	26	0.0028	0.00	0.00	0.00	0.00
N-NO_3-, mg/L	26	0.0155	0.01	0.01	0.00	0.03
S-SO_4^{2-}, mg/L	26	3.35	1.54	2.97	1.49	6.50
P-PO_4^{3-}, mg/L	18	0.0019	0.00	0.00	0.00	0.00
TBC, cells/mL	25	448680	383520	316930	59880	1341000
Li, µg/L	26	1.22	0.18	1.25	0.75	1.55
Be	26	0.0128	0.0029	0.0124	0.0086	0.022
B	26	9.58	2.81	8.63	3.30	17.4
Na	26	3411	1316	3580	1238	6526
Mg	26	2735	641	2706	1742	4120
Al	26	39.6	16.2	35.6	19.5	90.7
Si	26	1491	120	1501	1223	1780
P	26	5.55	2.09	4.9	3.1	10.8
K	26	530	238	432	338	1429
Ca	26	11160	4040	11040	6880	27380
Sc	26	0.0247	0.01	0.02	0.02	0.07
Ti	26	0.48	0.23	0.42	0.22	1.33
V	26	0.32	0.10	0.31	0.18	0.71
Cr	26	0.17	0.03	0.16	0.14	0.22
Mn	26	3.62	3.11	2.84	1.74	17.33
Fe	26	72.3	19.6	66.8	47.8	145
Co	26	0.056	0.03	0.05	0.03	0.15
Ni	26	0.54	0.29	0.45	0.33	1.76
Cu	26	1.30	0.78	0.95	0.73	4.50
Zn	26	70	160	25	4	835
Ga	26	0.03	0.01	0.03	0.02	0.08
As	26	0.16	0.05	0.17	0.09	0.34
Se	26	0.042	0.02	0.04	0.03	0.08
Rb	26	0.36	0.13	0.37	0.20	0.78
Sr	26	82.1	18.2	80.4	56.2	123.9
Y	26	0.17	0.05	0.17	0.10	0.34
Zr	26	0.12	0.08	0.11	0.06	0.51
Nb	26	0.0308	0.02	0.02	0.02	0.09
Mo	26	0.21	0.09	0.19	0.14	0.64
Cd	26	0.0199	0.02	0.01	0.01	0.10
Sn	25	0.33	1.12	0.04	0.00	5.52

Sb	26	0.029	0.01	0.03	0.01	0.07
Cs	26	0.0017	0.0007	0.0014	0.0008	0.0028
Ba	26	60.0	17.8	63.6	9.58	92
La	26	0.23	0.14	0.18	0.099	0.64
Ce	26	0.36	0.22	0.26	0.16	1.01
Pr	26	0.056	0.029	0.04	0.025	0.14
Nd	26	0.20	0.098	0.17	0.092	0.48
Sm	26	0.0435	0.016	0.04	0.022	0.086
Eu	26	0.0142	0.0025	0.01	0.010	0.019
Gd	26	0.0403	0.012	0.04	0.021	0.068
Tb	26	0.0055	0.0016	0.01	0.003	0.0089
Dy	26	0.0319	0.0093	0.03	0.017	0.055
Ho	26	0.0062	0.0018	0.01	0.0034	0.011
Er	26	0.0174	0.0052	0.02	0.0095	0.031
Tm	26	0.0024	0.0007	0.00	0.0014	0.0044
Yb	26	0.0162	0.0048	0.02	0.009	0.03
Lu	26	0.0024	0.0007	0.00	0.0013	0.0041
Hf	26	0.0890	0.049	0.08	0.049	0.31
W	26	0.0057	0.0025	0.01	0.0021	0.011
Tl	26	0.0015	0.0005	0.002	0.0007	0.003
Pb	26	0.090	0.038	0.08	0.05	0.19
Bi	26	0.0008	0.0002	0.00	0.0007	0.0013
Th	26	0.0309	0.024	0.02	0.0063	0.09
U	26	0.15	0.062	0.12	0.096	0.33

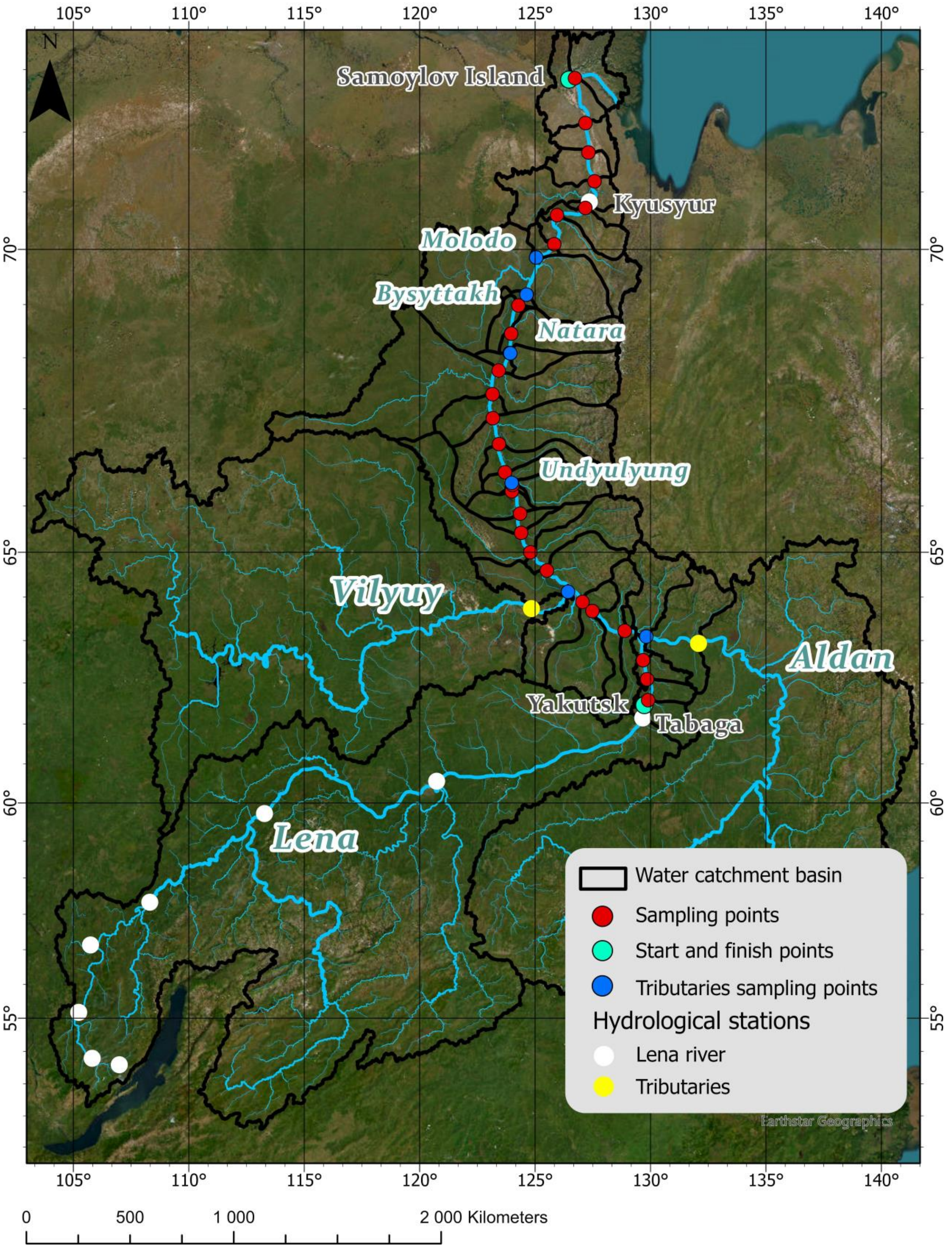

Fig. 1. A: The Lena River watershed and the position of sampling points of this study

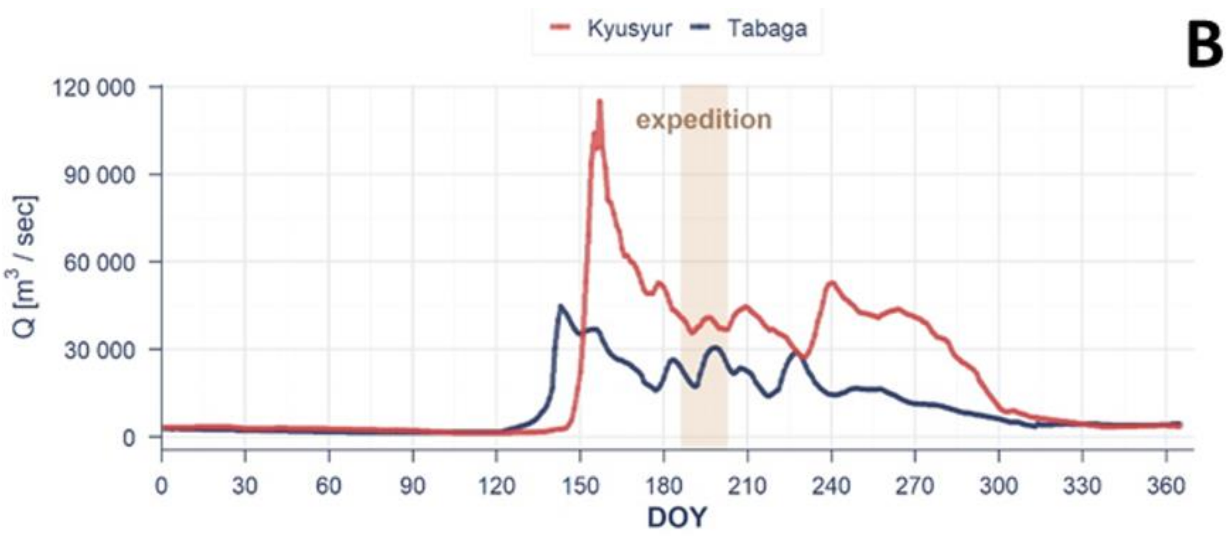

Fig. 1 B: Hydrograph of the Lena River at Kyusur (red line) and Tabaga (blue line) in 2022 for the period of expedition (highlighted in pink).

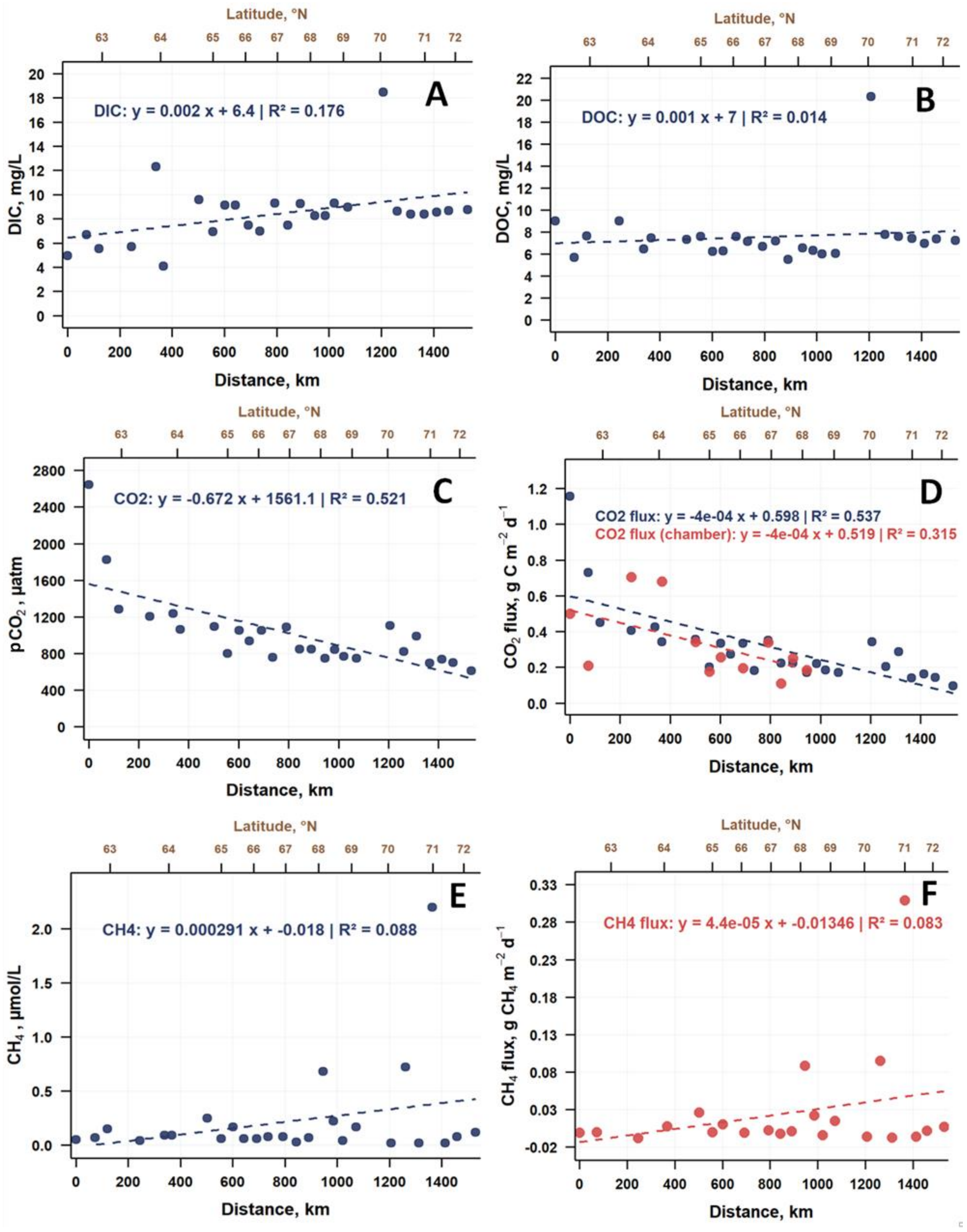

Fig. 2. Spatial variations of DIC (**A**), DOC (**B**), pCO_2 (**C**), FCO_2 (**D**), CH_4 concentration (**E**) and FCH_4 (**F**) in the main stem of the Lower Lena River, from Yakutsk to Kyusur. The dots represent discrete sampling points and dashed lines are linear regressions with equation parameters given on each panel.

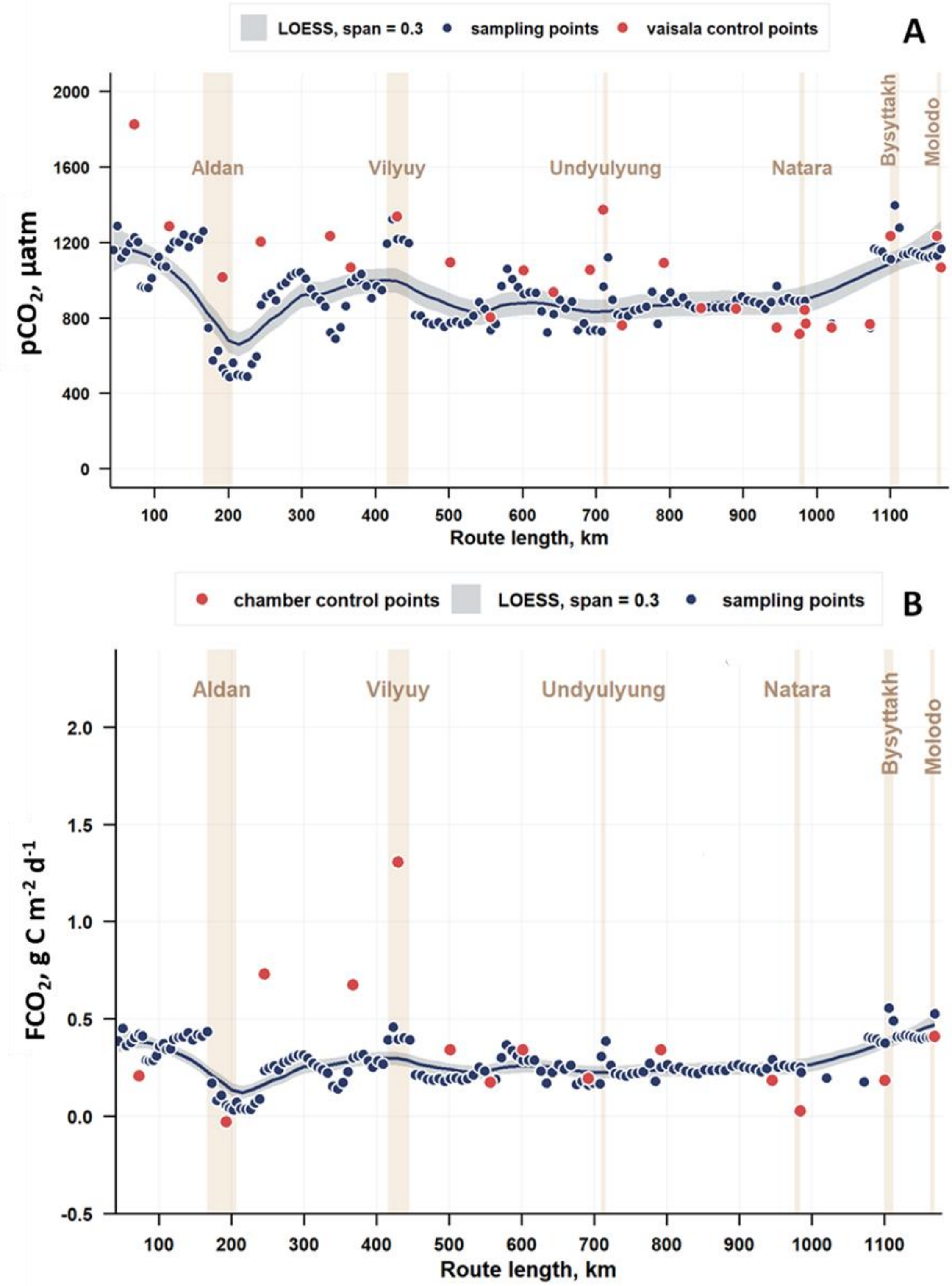

Fig. 3. Spatial variation of pCO_2 (**A**) and diffusive CO_2 flux (FCO_2) (**B**) along the Lower Lena River main stem during the south–north transect. Blue symbols show underway values obtained from the Kingston water intake, whereas red symbols show independent stationary checks obtained with a second Vaisala pCO_2 system. The two measurements were not strictly synchronous or spatially co-located; the red symbols therefore provide external field validation rather than exact replicate observations. Shaded vertical bands indicate the locations of major tributaries (Aldan, Vilyui, Undyulyung, Natara, Bysyttakh, Molodo). Solid lines represent LOESS (locally estimated scatterplot smoothing) fits: span = 0.3 for continuous measurements and span = 0.8 for control datasets due to their lower number of observations (*n* = 24).

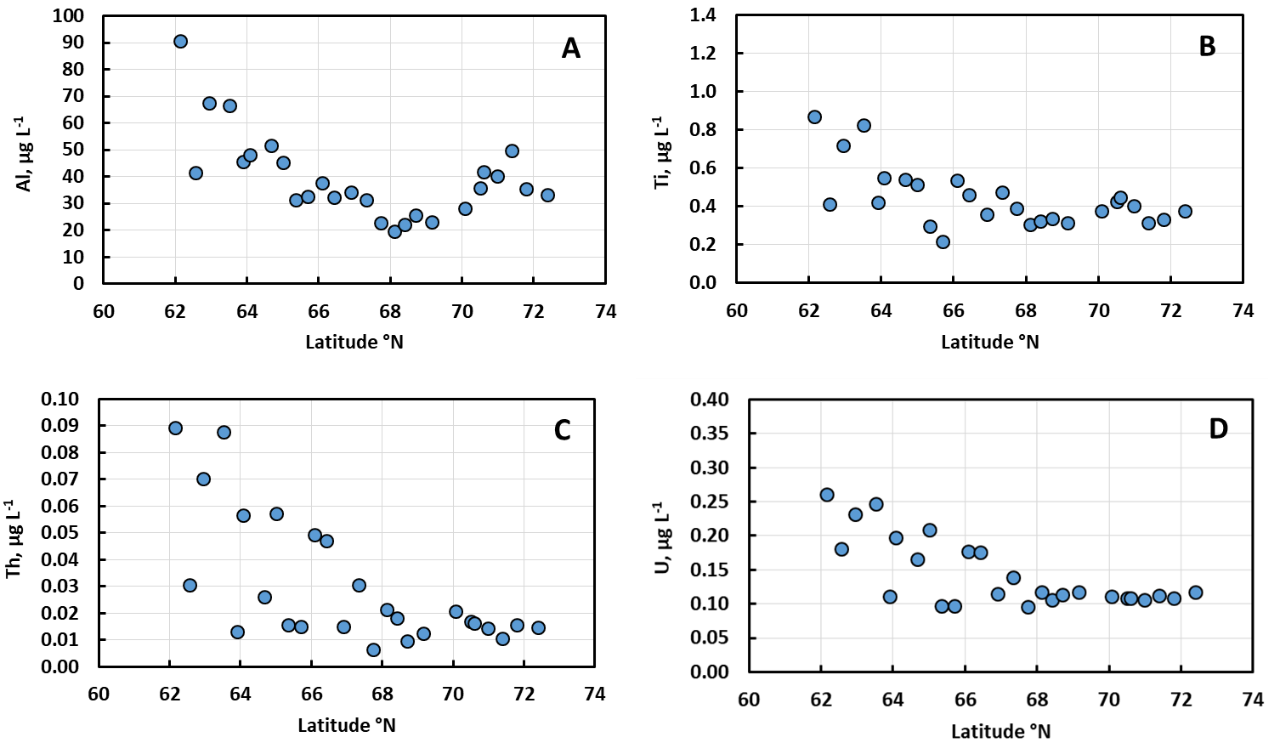

Fig. 4. Examples of low-solubility, predominantly colloidal elements whose concentration in the Lena River main stem decreased northward, from Yakutsk to Kyusyur: **A**, Al; **B**, Ti; **C**, Th and **D**, U.

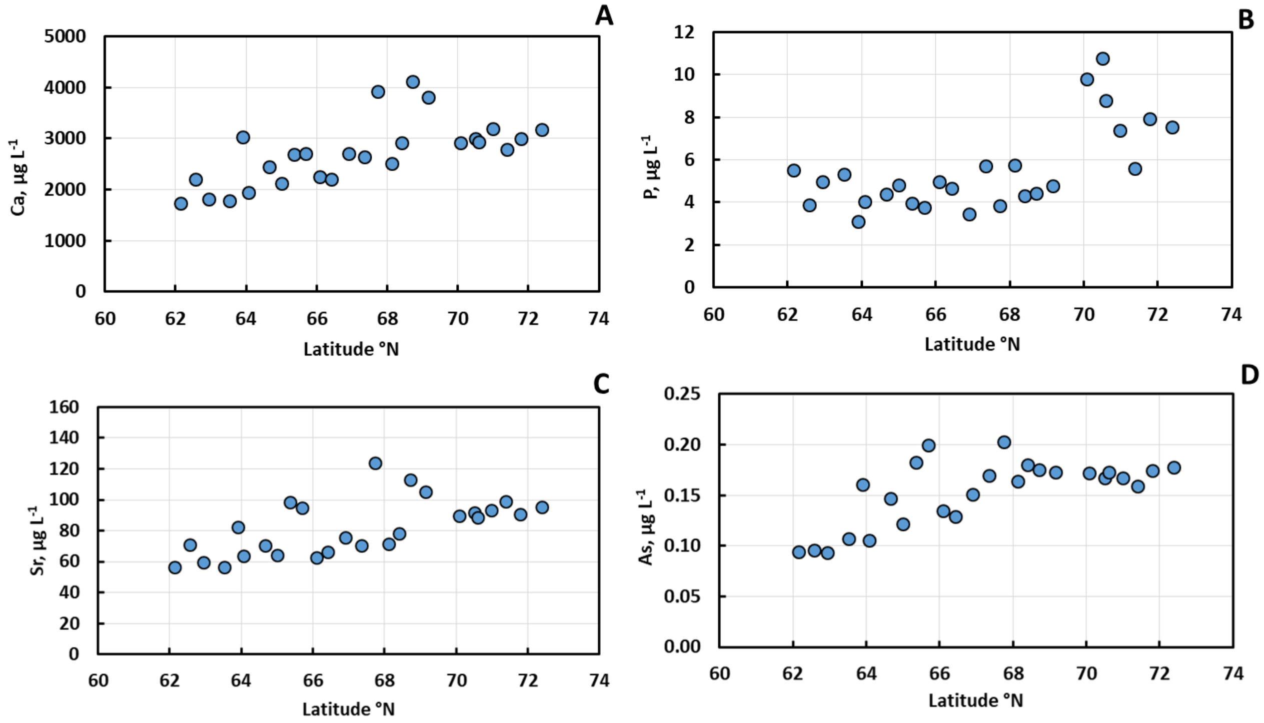

Fig. 5. Examples of labile elements with low colloidal proportions whose concentrations increased northward, from Yakutsk to Kyusyur: **A**, Ca; **B**, P; **C**, Sr and **D**, As.

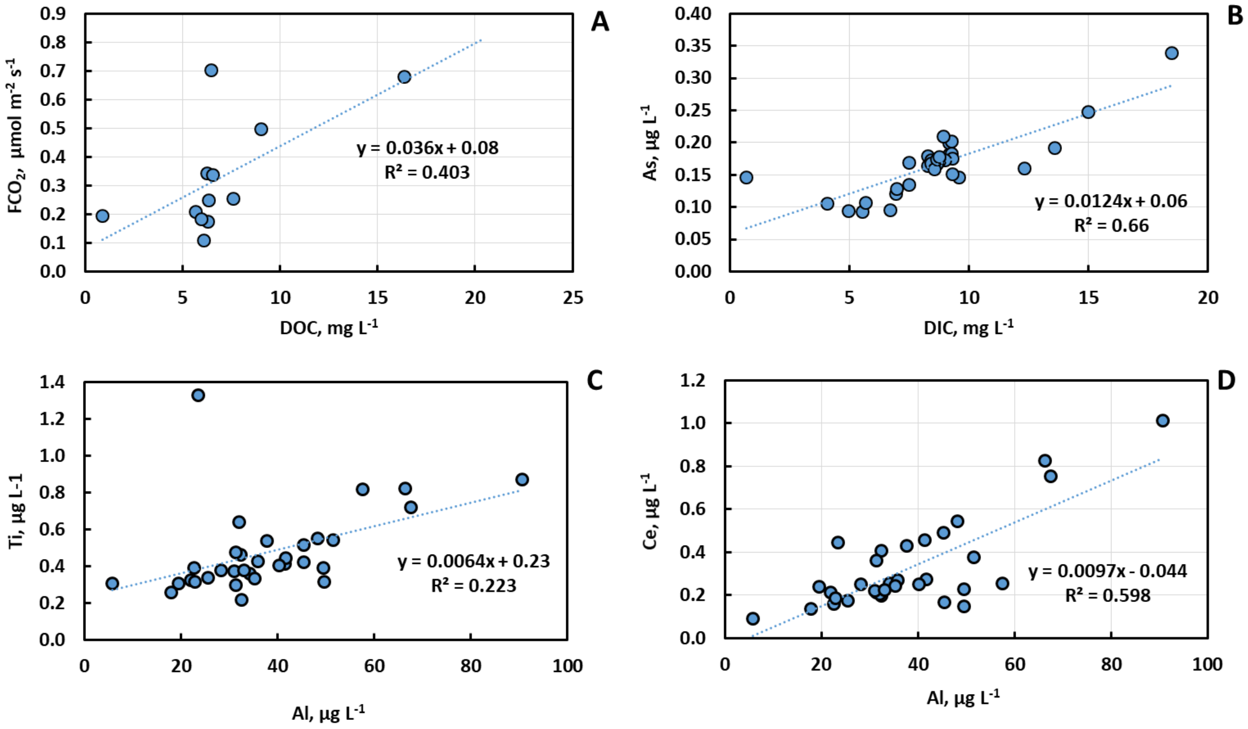

Fig. 6. Linear relationships in the Lena River main stem between concentrations of DOC and chamber-measured FCO_2 (**A**), DIC and As (**B**) and dissolved Al with Ti (**C**) and Ce (**D**).

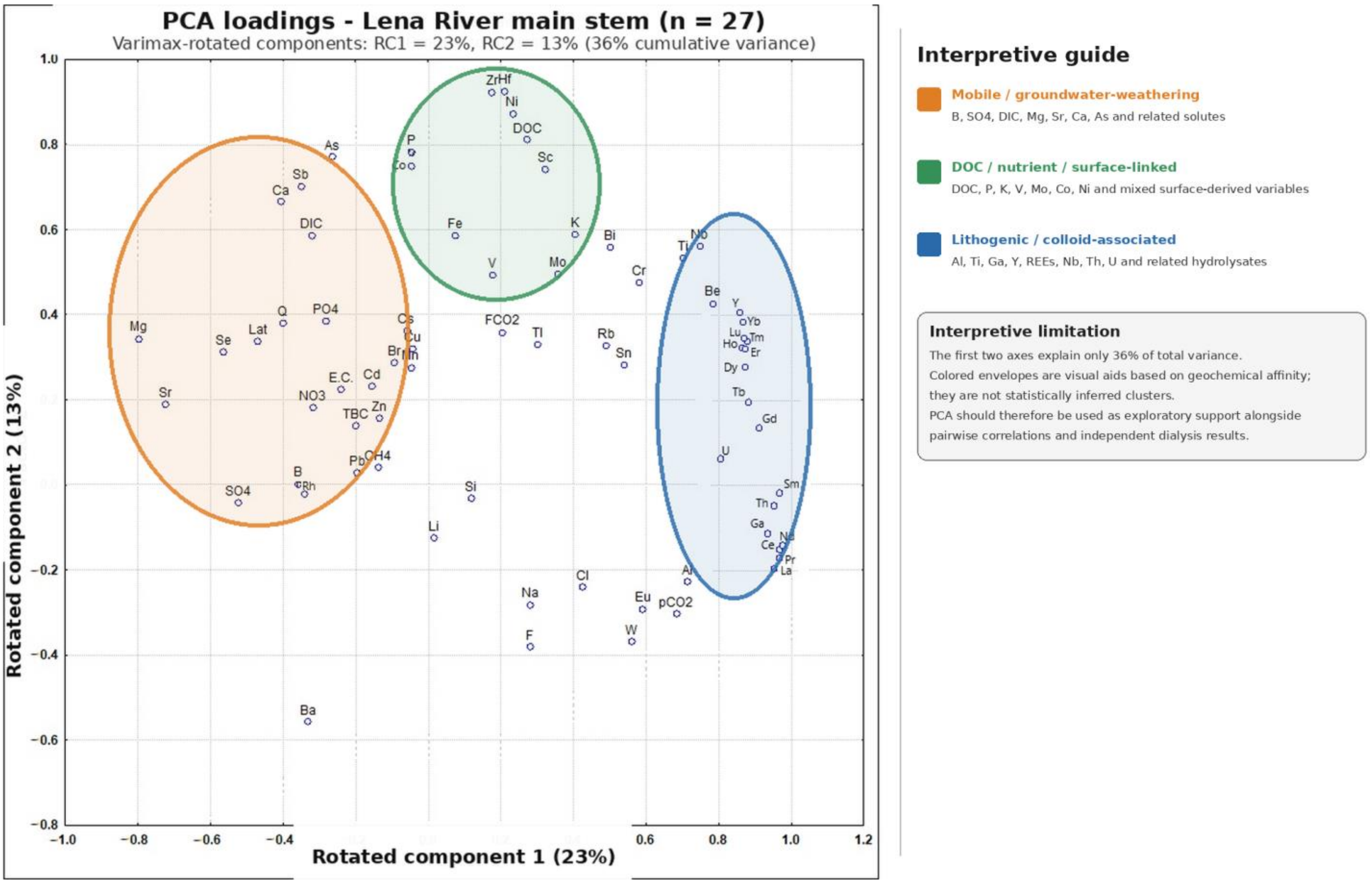

Fig. 7. Varimax-rotated PCA loading plot for standardized hydrochemical variables measured in the Lena River main stem (*n* = 26). Rotated components 1 and 2 explain 23% and 13% of total variance, respectively (36% cumulative). Colored envelopes are visual guides to broad geochemical associations inferred from the loadings and independent geochemical evidence: orange, mobile weathering- and groundwater-related solutes; green, DOC, nutrients, and mixed surface-derived variables; blue, low-solubility lithogenic and colloid-associated elements. Overlap among envelopes and variables outside them emphasize that the ordination is exploratory and does not represent statistically discrete clusters.

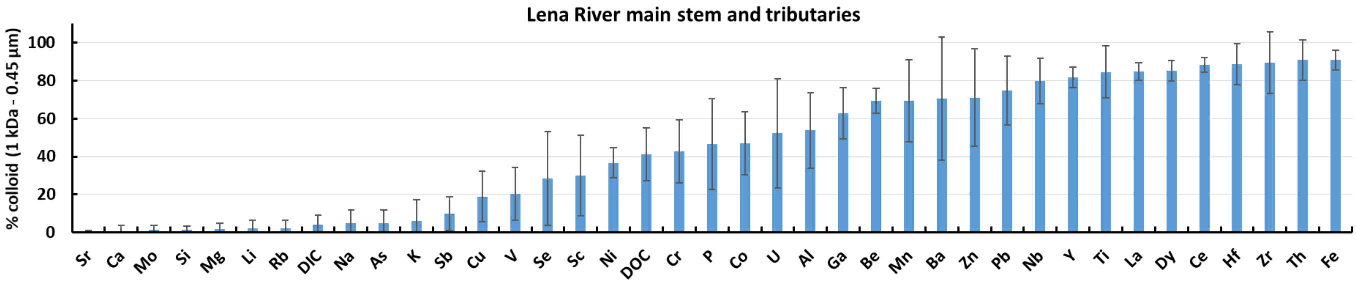

Fig. 8. Average (± s.d., n = 12) proportion of colloidal forms of major and trace elements in the Lena River and tributaries measured by dialysis procedure.